nature medicine

Article

https://doi.org/10.1038/s41591-025-03885-3

# Patritumab deruxtecan in HR$^+$HER2$^-$ advanced breast cancer: a phase 2 trial

Received: 31 March 2025

Accepted: 3 July 2025

Published online: 04 September 2025

Check for updates

A list of authors and their affiliations appears at the end of the paper

Antibody–drug conjugates have shown impressive clinical outcomes, particularly in metastatic breast cancer, but biomarkers to predict response and resistance remain unidentified. Here we report the results of ICARUS-BREAST01, a phase 2 study evaluating efficacy, safety and biomarkers of response and resistance to patritumab deruxtecan (HER3-DXd), in patients with HR$^+$HER2$^-$ metastatic breast cancer, who previously progressed on CDK4/6 inhibitors and one line of chemotherapy. From May 2021 to June 2023, 99 patients were enrolled to receive HER3-DXd 5.6 mg kg$^{-1}$ intravenously every 3 weeks. The study met its primary endpoint, showing an overall response rate of 53.5% (90% confidence interval [44.8–62.1%]). The most frequent adverse events were fatigue (83%), nausea (75%), diarrhea (53%) and alopecia (40%). Exploratory biomarker analysis of baseline tumor samples suggested preliminary associations between overall response rate and both HER3 spatial distribution and absence of estrogen receptor 1 (ESR1) mutations, as well as between progression-free survival and HER3 expression, pending further validation. Analysis of on-treatment tumor samples showed that treatment efficacy seems to be associated with antibody–drug conjugate intratumoral distribution and interferon response. Overall, HER3-DXd showed promising activity and manageable tolerability in patients with HR$^+$HER2$^-$ metastatic breast cancer who progressed on CDK4/6 inhibitors. These findings highlight the need for larger trials to define HER3-DXd efficacy relative to other drugs, including antibody–drug conjugates (ClinicalTrials.gov Identifier: NCT04965766).

Breast cancer remains the most frequent cancer in women, with 2.3 million new cases and 685,000 deaths worldwide in 2020 (refs. 1,2). There is therefore an urgent need to develop new therapeutic agents for this disease. Antibody–drug conjugates (ADCs) are complex compounds that combine a tumor-targeting antibody with a cytotoxic or bioactive payload via a chemical linker. The antibody binds to a membrane protein (target) that leads to the ADC internalization and ultimately to the payload release upon cleavage in the endosomal or lysosomal system[3]. However, as it has been estimated that only a small proportion of the drug reaches the tumor cells, the mechanism of action of ADCs is likely to extend beyond payload delivery, with additional mechanisms contributing to their efficacy, such as the antibody-dependent cellular cytotoxicity, complement-dependent cytotoxicity and immunogenic cell death[4–6]. Furthermore, it has been shown that both the bystander effect and the systemic release of the payload, related to either linker–drug instability or antibody–linker instability, can also determine ADC activity across tumor cells with a wide range of target expression[7–9]. ADCs have ushered in a new era in oncology, by providing unprecedented results in both solid tumors and hematological malignancies. Trastuzumab deruxtecan (T-DXd) has substantiallyimproved survival outcomes in patients with HER2 (also known as ERBB2)-expressing breast cancer (HER2$^+$ and HER2-low)[10,11]. Similarly, sacituzumab govitecan and datopotamab deruxtecan (HER3-DXd) have demonstrated remarkable efficacy in HER2-low and HER2-0 breast

e-mail: barbara.pistilli@gustaveroussy.fr

cancers[12,13]. However, there remains room to develop new ADCs and combination strategies to expand the range of targetable antigens, enhance safety profiles and further personalize ADC selection based on patient and tumor characteristics, ultimately broadening the therapeutic landscape.

Furthermore, reliable biomarkers for identifying patients most likely to obtain clinical benefit from ADC therapies remain an unmet medical need and the mechanisms of action of ADCs are still not well understood[4,5]. This is due to the limited number of clinical trials that systematically perform baseline (BL) and on-treatment tumor biopsies to understand ADC mechanisms of action and resistance. Such serial tumor biopsy was performed in the DAISY trial, which showed that response to T-DXd was associated with human epidermal growth factor receptor-2 (HER2) spatial distribution and the level of drug internalization was correlated with the expression of HER2 (ref. 14). Nevertheless, the impact of ADC intratumoral distribution on treatment outcome, along with the underlying mechanisms of action of most ADCs in patients, remains largely unknown. To address these gaps, we developed the ICARUS-BREAST01 study[15]. This academic, phase 2 trial aimed to evaluate clinical efficacy, safety and biomarkers of response and resistance to HER3-DXd, in patients with $HR^{+}HER2^{-}$ advanced breast cancer, who previously progressed on CDK4/6 inhibitors and endocrine therapy and received one line of chemotherapy. In hormone receptor-positive ($HR^{+}$) and $HER2^{-}$ advanced breast cancer, endocrine therapy with CDK4/6 inhibitors has significantly improved disease and survival outcomes and several effective therapeutic agents are available beyond progression, particularly PI3K–AKT–mTOR pathway inhibitors in combination with endocrine therapy[16–19]. However, about 50% of patients receiving CDK4/6 inhibitors experience disease progression over the first 2 years of treatment and become rapidly eligible for standard chemotherapy, which is often associated with significant toxicity[20,21]. In breast cancer, HER3 expression plays a key role in resistance to PI3K–AKT–mTOR inhibitors, HER2-targeting therapies and endocrine therapy and is associated with poorer prognosis[22]. HER3-DXd is a new ADC composed of an anti-HER3 monoclonal antibody conjugated to a topoisomerase-I inhibitor by a cleavable peptide linker, which has shown preliminary signs of activity regardless of breast cancer subtype and HER3-expression in earlier phase 1 and 2 studies[23].

## Results

### Patients' characteristics

From 27 May 2021 to 9 March 2023, we screened 164 patients with estrogen receptor-positive ($ER^{+}$) and/or progesterone receptor-positive ($PR^{+}$) and $HER2^{-}$ (immunohistochemistry (IHC) 2+ and in situ hybridization (ISH) negative, or IHC 1+ or IHC 0+), unresectable locally advanced or metastatic breast cancer, who had progressed on previous treatment with CDK4/6 inhibitors and endocrine therapy and received one line of chemotherapy for advanced breast cancer. A total of 99 patients were enrolled to receive HER3-DXd 5.6 mg $kg^{-1}$ intravenously (i.v.) every 3 weeks until progression or unacceptable toxicity (Fig. 1). The study primary endpoint was the confirmed objective response rate (ORR) by a local investigator, whereas secondary endpoints included progression-free survival (PFS), duration of response (DoR), overall survival (OS) and safety. To explore biomarkers of response or resistance to HER3-DXd, we collected one frozen and three formalin-fixed paraffin-embedded (FFPE) tumor samples at BL, on-treatment (corresponding with cycle 1 day 3 (C1D3), cycle 1 day 19 (C1D19) or cycle 2 day 3 (C2D3)) and at end of treatment, along with whole-blood and serum samples. The main demographic and clinical characteristics of patients at study entry are reported in Table 1. Overall, 39.4% of patients had IHC HER2-0 breast cancer, as centrally assessed on the tumor biopsy at study entry. The median number of systemic therapies for advanced breast cancer was two (range one to four). All patients, with the exception of one, had progressed on previous CDK4/6 inhibitor with a median treatment duration of 13.7 months (interquartile range (IQR) 6.5–19.7 months). At data cut-off, 16 April 2024, 19 patients were still on treatment and the median number of treatment cycles was 11.0 (IQR 6–18.0), with disease progression being the primary reason for treatment discontinuation in most patients (64.6%), as reported in Supplementary Table 1.

### Efficacy

The confirmed ORR by the local investigator was 53.5% (90% confidence interval (CI) [44.8–62.1%]), with 2 patients having obtained complete response (CR) and 51 partial response (PR). Overall, 37 patients had stable disease (SD), with a clinical benefit rate (CBR) (CR, PR or SD ≥ 6 months) of 62.6% (95% CI [52.3–72.1%]) (Fig. 2a).

With a median duration of the study follow-up of 15.3 months (95% CI [13.0–17.2 months]), 62 patients experienced disease progression or death. The median PFS as assessed by the local investigator was 9.2 months (95% CI [8.0–12.8 months]) (Fig. 2b). The median DoR was 9.3 (95% CI [8.15–not available (N/A)) months] (Fig. 2c). OS was not mature at the time of data cut-off.

We also performed a post-hoc analysis of ORR and PFS according to HER2 expression as centrally assessed on the tumor biopsy at BL and we found an ORR of 60% (95% CI [40.6–77.3%]) in the HER2-low (1+, 2+) and of 48.7% (95% CI 32.4–65.2%) in the HER2-0 patient populations. Median PFS was 12.8 (95% CI [8.11–N/A]) months and 9.1 (95% CI 6.7–N/A) months in HER2-low and HER2-0, respectively (Supplementary Table 2a,b,c and Supplementary Fig. 1). Given the high ORR observed by the local investigator assessment, the study was also amended in November 2024 to include a retrospective independent central review of RECIST, which confirmed an ORR of 55.6% (95% CI [45.2–65.5%]).

### Safety

The median duration of treatment at data cut-off was 251.0 d (range 144.5–402.0 d). Treatment-related adverse events (TRAEs) of any grade occurred in 97 patients (98.0%) and the rate of grade ≥3 TRAEs was 50.1%. Serious TRAEs were reported in 18.2% of patients. TRAEs led to dose reductions in 20 patients (20.2%), dose interruptions in 22 patients (22.2%) and HER3-DXd discontinuation in 11 patients (11.1%). No fatal TRAEs were reported, although one patient died while on treatment due to a massive pleural effusion not related to HER3-DXd. The most frequent TRAEs of any grade (>30% of patients) were: fatigue (83%), nausea (75%), diarrhea (53%) and alopecia (40%). Any grade treatment-related thrombocytopenia was reported in six patients, of whom two had a grade 3 and three a grade 4. The most common TRAEs and the most common treatment-emergent adverse events (TEAEs) are reported in Table 2. Note that the study protocol recommended systemic prophylaxis with a serotonin 5-HT3 antagonist in all patients and the use of an additional antiemetic as indicated per the investigator's discretion. AEs of special interest (AESIs) were reported in 15 patients: eye disorders of any grade occurred in 10 patients and were mostly low grade (grade 1: 5 patients; grade 2: 3 patients; grade 3: 2 patients). Throughout the conduction of the study, 10 patients (10.1%) experienced interstitial lung disease (ILD) or suspicion of ILD attributed to the study treatment by the local investigator, of which 7 were grade 1 and 3 grade 2. Eight patients had adjudicated HER3-DXd-related ILD, as determined by an independent ILD adjudication committee. Most cases ($n = 6$) were classified as grade 1, with one leading to study drug discontinuation at the investigator's decision and two were grade 2, both resulting in treatment discontinuation as per protocol. Treatment was required in four of the grade 1 cases and in both grade 2 cases. Among the six patients with available data on ILD duration, two cases resolved within approximately 3 weeks, two cases within 1 month and two cases required around 6 months for resolution.

### BL predictors of response to HER3-DXd

One of the primary objectives of the exploratory analysis of the ICARUS-BREAST01 study was to identify predictors of treatment

https://doi.org/10.1038/s41591-025-03885-3

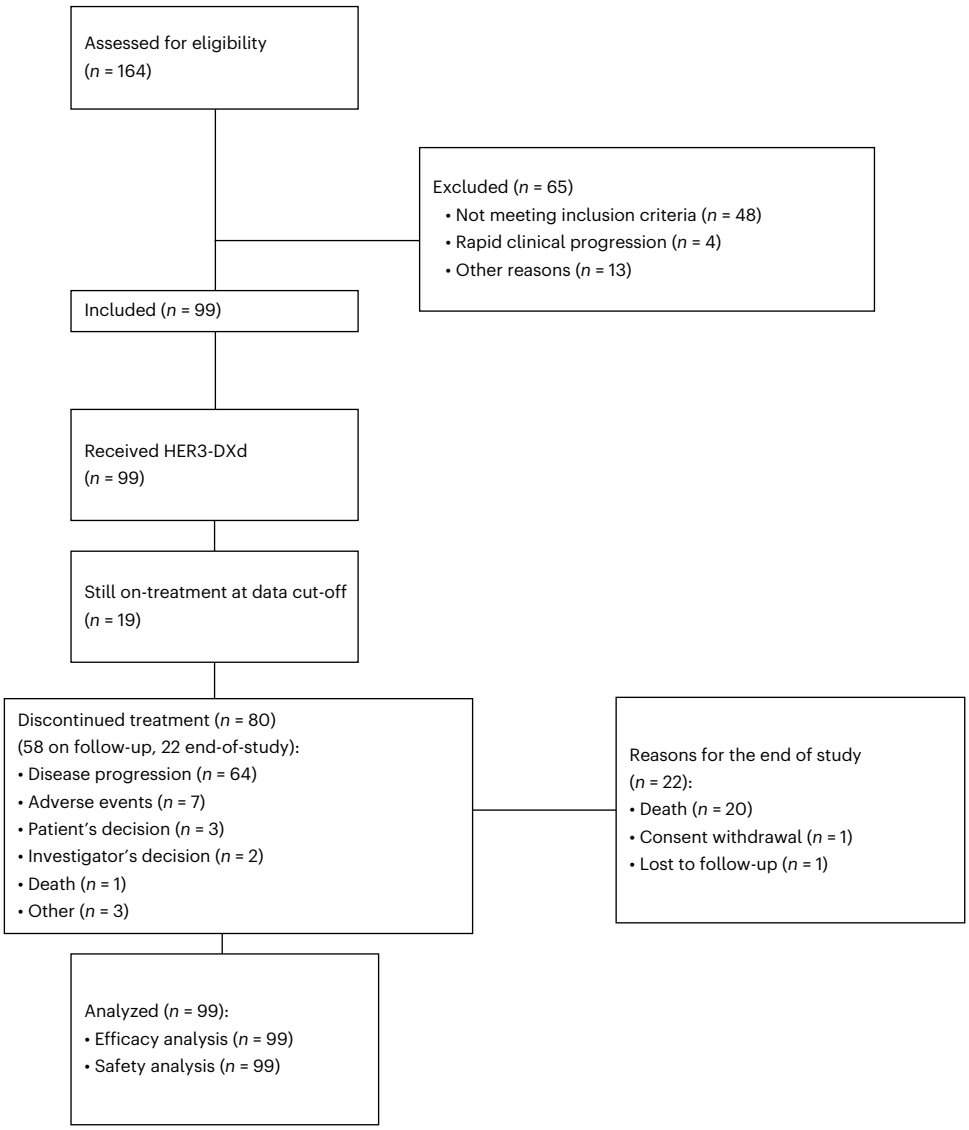


**Fig. 1 | Study consort diagram.** CONSORT flowchart illustrating patient disposition throughout the study.

response using tumor samples collected at BL. We defined the patients as responders if they achieved a confirmed CR or PR and as nonresponders if their best response was SD or progressive disease (PD). We first investigated whether the target expression and spatial distribution were associated with treatment outcome (ORR or PFS). Therefore, we evaluated membrane HER3 expression, on FFPE tumor samples at BL ($n = 72$), as measured by overall membrane positivity at ×10 magnification and membrane *H*-score. Although the HER3-expression prescreening was removed by amendment on 15 April 2022, after the inclusion of the first 29 patients, most patients ($n = 49$ of 72 (68%)) had ≥75% of HER3-membrane positivity and only 22% ($n = 16$ of 72) had <25%, with a median of 82.5 (range 0–100) (Table 1). We found a slightly greater ORR in patients with HER3-membrane positivity >25%, with the ORR 43.8% (95% CI [19.8–70.1%]) in the group with <25% ($n = 16$), 85.7% (95% CI [42.1–99.6%]) in the group with 25–75% ($n = 7$) and 51.0% (95% CI [36.3–65.6%]) in the group with >75% ($n = 49$). Conversely, we did not find a meaningful difference in the ORR across the HER3-membrane expression as measured by the *H*-score (Extended Data Fig. 1). Analysis of PFS according to HER3-membrane expression showed a trend toward a slightly longer PFS in patients with HER3-membrane positivity >75% (median(m)PFS 10.9 months (95% CI [8.2–17.7 months]) or with HER3-membrane *H*-score >200 (mPFS 10.9 months (95% CI [8.51 months–N/A]) compared with those with the lowest HER3-membrane scoring (mPFS 8.1 months (95% CI [4.4 months–N/A]) in HER3-membrane positivity <25%; mPFS 6.7 (95% CI [5.3 months–N/A]) in HER3-membrane *H*-score 0–100) (Extended Data Fig. 1). Developing these results further, we performed a post-hoc analysis of ORR and PFS using the HER3-membrane IHC scoring 1+, 2+ and 3+ as previously reported in ref. 23 and selected the top IHC algorithms and cutoffs (percentage of tumor cells (%TC) with membrane 2+ and 3+ ≥50%, %TC membrane 1+, 2+ and 3+ ≥75%). Consistent with earlier analysis, we did not find a statistically significant association between ORR and HER3-membrane positivity; however, we observed a trend for longer PFS in patients with %TC membrane 2+ and 3+ ≥50% versus <50% (9.7 months (95% CI [8.1–15.3] months) versus 6.8 months (95% CI [5.3 months–N/A]; $P = 0.126$)) and in those with %TC membrane 1+, 2+ and 3+ ≥75% versus <75% (10.9 months (95% CI [8.1–17.6 months]) versus 8.1 months (95% CI [6.7 months–N/A]); $P = 0.136$; Fig. 3a,b). Nevertheless, the correlative analysis of HER3 versus efficacy should be interpreted with caution, because the limited sample size results in wide CIs. We also analyzed the correlation between HER2 and HER3 expression by IHC to determine whether their expression is associated. We did not observe any clear correlation between HER3 and HER2 expression. Indeed, tumors with ≥50% $HER3^{+}$ membrane staining were found across both HER2-0 and HER2-low groups (Supplementary Fig. 2).

https://doi.org/10.1038/s41591-025-03885-3

**Table 1 | Characteristics of patients and tumors at baseline (*n*=99)**

| | |
|---|---|
| **Age** | |
| Median (range), years | 57.0 (48.0–66.0) |
| Sex, *n* (%) | |
| Female | 99 (100.0) |
| **ECOG PS, *n* (%)** | |
| 0 | 56 (56.6) |
| 1 | 40 (40.4) |
| N/A | 3 (3.0) |
| **Menopausal status, *n* (%)** | |
| Premenopausal | 23 (23.2) |
| Postmenopausal | 75 (75.8) |
| N/A | 1 (1.0) |
| **Stage at initial tumor diagnosis, *n* (%)** | |
| I | 13 (13.1) |
| II | 19 (19.2) |
| III | 11 (11.1) |
| IV | 30 (30.3) |
| N/A | 26 (26.3) |
| **HR status at initial tumor diagnosis, *n* (%)** | |
| $ER^+PR^+$ | 76 (76.8) |
| $ER^+PR^-$ | 18 (18.2) |
| $ER^-PR^-$ | 1 (1.0) |
| N/A | 3 (3.0) |
| **HER2 expression at initial tumor diagnosis, *n* (%)** | |
| IHC 0 | 56 (56.6) |
| IHC 1+ | 22 (22.2) |
| IHC 2+, ISH nonamplified | 11 (11.1) |
| IHC 2+, ISH amplified | 1 (1.0) |
| Unknown | 9 (9.1) |
| **HER2 expression on tumor biopsy at baseline, *n* (%)** | |
| IHC 0[a] | 39 (39.4) |
| IHC 1+ | 22 (22.2) |
| IHC 2+, $ISH^-$ | 7 (7.1) |
| IHC 3+ | 1 (1.0) |
| Unknown | 30 (30.3)[b] |
| **HER3 expression** | |
| **Membrane *H*-score, median (range)** | 180 (0–290) |
| **Overall membrane positivity at 10×, *n* (%)** | |
| <25% | 16 (16.2) |
| 25–74% | 7 (7.1) |
| ≥75% | 49 (49.4) |
| Unknown | 27 (27.3) |
| **Metastatic sites at study entry, *n* (%)** | |
| Liver | 60 (60.6) |
| Lung | 8 (8.1) |
| Nodes | 9 (9.1) |
| Brain | 0 (0) |
| **Median number of systemic therapies for ABC, *n* (range)** | 2 (1–4) |
| **Previous treatment with CDK4/ 6inh, *n* (%)** | 98 (99.0)[c] |
| **Median duration of CDK4/6inh, months (range)** | 13.7 (2.9–42.0)[d] |
| **Previous PI3K–AKT–mTOR inh for ABC, *n* (%)** | 35 (35.4) |
| **Previous chemotherapy for ABC, *n* (%)** | 99 (100.0) |
| **Type of chemotherapy for ABC, *n* (%)** | |
| Capecitabine | 53 (53.6) |
| Taxanes | 23 (23.2) |
| Others | 23 (23.2) |

[a]20 with HER2 membrane staining 1–10%. [b]Insufficient tumor tissue available. [c]96 patients had CDK4/6inh for ABC, 2 patients for early breast cancer; 1 patient was enrolled by mistake because did not receive any previous treatment with CDK4/6inh. [d]Evaluated on 73 patients. ECOG, Eastern Cooperative Oncology Group.

We further explored whether the spatial distribution of $HER3^+$ cells was associated with response to the treatment. After the pathologist's review, we analyzed 69 IHC or hematoxylin and eosin (H&E) slides. First, we performed machine learning analysis on digitized, annotated, DAB-stained slides (membrane HER3 expression) by using an unsupervised clustering algorithm, as previously done in the DAISY trial[14]. Using two different models to extract patch representations, we did not find any significant association between the identified clusters and response to HER3-DXd. Afterwards, to map the distribution of $HER3^+$ cells relative to neighboring cells, we superimposed digitized, whole DAB-stained slides with digitized H&E-stained slides from the same sample, capturing the architecture of the tumor microenvironment (TME) ($n = 63$, because 6 samples were excluded as a result of suboptimal registration quality control). We developed a new pipeline to identify epithelial, connective, inflammatory and necrotic areas, together with $HER3^+$ and $HER3^-$ areas (Methods). These regions were then segmented into eight different clusters, the proportion of which was compared between responders and nonresponders. Our analysis revealed an association between treatment response and the percentage of cluster 0 (odds ratio (OR) 1.527; 95% CI [1.020–2.287]; $P = 0.040$; Fig. 3c and Supplementary Fig. 5). According to the pathologist's review, cluster 0 was characterized by isles containing a moderate number of $HER3^+$ cells, surrounded by connective areas enriched with blood vessels, with few immune cells and no necrotic areas (Fig. 3d,e). To explore whether cluster 0 was associated with better tumor vascularization, we used ERG (ETS-related gene) IHC staining to selectively identify endothelial cells. We found a significant positive association between cluster 0 and number of $ERG^+$ cells ($P = 0.0275$; Supplementary Fig. 3); however, this association did not remain significant after multiple testing correction and should be interpreted with caution. We further evaluated the proportion of cluster 0 in tumor samples collected at progression and we did not find any statistically significant difference in the proportion of cluster 0 at baseline and that at progression; however, these results should be interpreted with caution because only 11 tumor samples were analyzable at disease progression (Supplementary Fig. 4). By training the clustering algorithm without incorporating DAB information, we also found that cluster 0* and cluster 1* were associated with response to the treatment (OR 1.48 and 1.58 and $P = 0.029$ and 0.014, respectively). Although cluster 0* was composed of only connective tissue and so lacked biological rationale, cluster 1* seemed to share similar properties with the previously identified cluster 0, featuring TCs surrounded by connective areas, few immune cells and no necrotic areas (Supplementary Fig. 6). Next, we analyzed whether genomic alterations at BL were associated with response to HER3-DXd. We carried out whole-exome sequencing (WES) on frozen tumor biopsies at BL ($n = 43$). Nonsynonymous point mutations, insertions or deletions (indels), homozygous deletions, loss of heterozygosity and low, medium and high-level amplifications were

https://doi.org/10.1038/s41591-025-03885-3

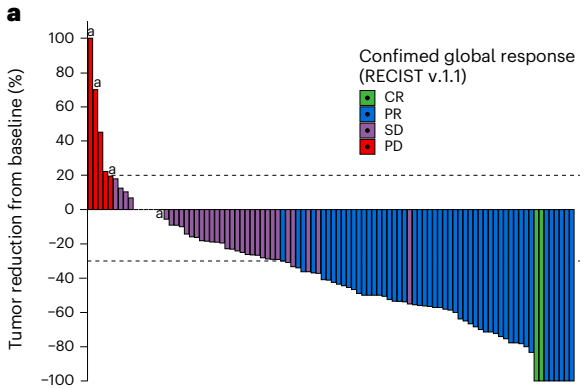


| Confirmed response | *n* = 99 | Percentage | 90% CI[b] |
|---|---|---|---|
| Overall ORR | 53 | 53.5 | [44.8–62.1] |
| CR | 2 | 2 | [0.4–6.2] |
| PR | 51 | 51.5 | [42.8–60.2] |
| SD | 37 | 37.4 | [29.2–46.1] |
| PD | 7 | 7.1 | [3.4–12.9] |
| NE[c] | 2 | 2 | [0.4–6.2] |

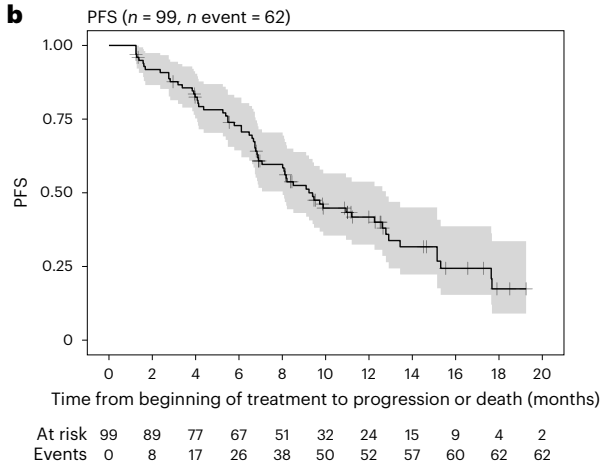


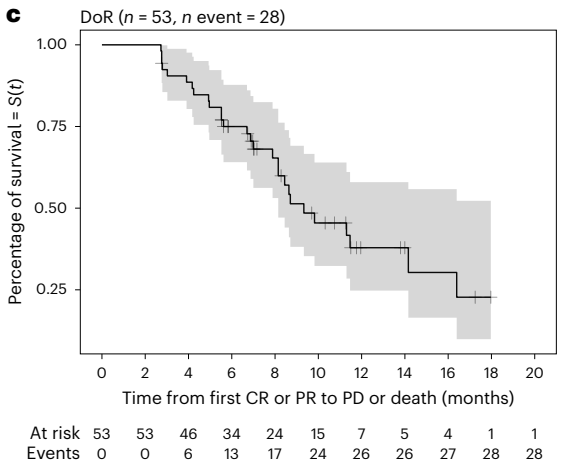


**Fig. 2 | Efficacy of HER3-DXd. a**, Waterfall plot showing the best percentage change in the sum of tumor diameters from BL. The bars colored green, blue, purple and red represent CR, PR, SD and PD, respectively. The response was determined by investigator assessment according to RECIST v.1.1 and required confirmation after the first observed response at least 4 weeks later. The Clopper–Pearson (exact) method was used for the CIs. **b**, Kaplan–Meier estimates of PFS as assessed by a local investigator (median 9.2 months (95% CI [8.0–12.8 months]). **c**, Kaplan–Meier estimates of duration of response as assessed by a local investigator (median 9.3 months (95% CI 8.2 months–N/A)). [a]Patients who developed new lesions; [b]Clopper–Pearson (exact) method used for the 90% CI; [c]two patients not evaluable (NE) for ORR: one patient had only one tumor assessment with PR and then treatment discontinued due to clinical progression and a second patient had no evaluable global response-of-target lesions.

assessed. A set of 73 genes of interest was selected before the start of the project (Methods). Analyses of WES were focused on these genes (Supplementary Table 3). *TP53* alterations were observed in 53.8% (14 of 26) and 29.4% (5 of 17) and *PIK3CA* alterations in 38.5% (10 of 26) and 17.6% (3 of 17) of responders and nonresponders, respectively.

It is interesting that we found a higher proportion of *ESR1* mutations in nonresponders 52.9% (9 of 17) compared with responders 23.1% (6 of 26), with all 4 patients with PD as best response presenting *ESR1* alterations at baseline. *ERBB3* mutations were detected in 11.5% (3 of 26) of responders versus 5.9% (1 of 17) of nonresponders, with 2 of 3 mutations found in responders that were ranked as likely pathogenic according to OncoKB. Finally, we found a higher frequency of *FGFR1* amplifications (5 high, 3 medium and 1 low level) in responders, 34.6% (9 of 26), including the 2 patients with a confirmed and prolonged CR, compared with nonresponders, 23.5% (4 of 17) (Extended Data Fig. 2a). WES analysis according to the CBR, as defined by CR, PR or SD ≥ 6 months confirmed the same results (Extended Data Fig. 2b). We also performed the analysis of 21 mutational signatures with activity in at least 2% of breast cancer samples, showing an association between APOBEC-related SBS2 and treatment response (Supplementary Fig. 7). Next we investigated the association between gene expression at BL and PFS, by performing bulk RNA sequencing (RNA-seq) on 56 BL frozen tumor biopsies. The adaptive lasso model procedure led a five-gene model for prediction of PFS, which contained *RAB40AL*, *MAGEB17* and *MKRN7P* ($P < 0.05$). Note that RAB4 proteins are localized in early endosomes and regulate early endosomal recycling, determining a fast transport of internalized receptors from the endosomes back to the plasma membrane[24]. Therefore, the association of higher expression of RAB4 with poor prognosis suggests that higher recycling of internalized HER3-DXd back to the plasma membrane is detrimental to its efficacy (Supplementary Fig. 8). Finally, given the higher proportion of *ESR1mut* (mutated) in nonresponders, we tried to better characterize the *ESR1mut* and *ESR1wt* (wild-type) group. We found that the median number of genomic alterations along with tumor mutational burden were similar in the two groups (Supplementary Table 4). We also compared the proportion of luminal tumors in the *ESR1mut* and *ESR1wt* groups, by performing PAM50-intrinsic subtyping on available bulk RNA-seq data ($n = 14$ *ESR1mut*, $n = 23$ *ESR1wt*) and we did not find any difference between the two groups ($\chi^2$ test, $P = 0.57$) (Supplementary Table 4). Nevertheless, gene set enrichment analysis (GSEA) using the Hallmark gene sets showed activation of estrogen pathways in *ESR1mut* compared with *ESR1wt* tumors (Supplementary Fig. 9).

## Mechanisms of action and pharmacodynamics of HER3-DXd

We also aimed to evaluate the potential mechanisms of action of HER3-DXd and determine whether distinct mechanisms of action or pharmacodynamic events could explain treatment response. For this purpose, we analyzed tumor samples collected at BL and during

https://doi.org/10.1038/s41591-025-03885-3

**Table 2 | Safety profile**

| | Any grade, *n* (%) | Grade ≥3, *n* (%) |
|---|---|---|
| TRAEs occurring in ≥10% of patients | | |
| Fatigue | 82 (82.8) | 10 (10.1) |
| Nausea | 74 (74.7) | 14 (14.1) |
| Diarrhea | 52 (52.5) | 10 (10.1) |
| Alopecia | 40 (40.4) | 0 |
| Constipation | 21 (21.2) | 0 |
| Vomiting | 18 (18.2) | 3 (3.0) |
| Anorexia | 16 (16.2) | 1 (1.0) |
| Neutrophil count decrease | 14 (14.1) | 12 (12.1) |
| Abdominal pain | 11 (11.1) | 0 |
| Stomatitis | 10 (10.1) | 0 |
| Anemia | 10 (10.1) | 0 |
| TEAEs occurring in ≥10% of patients | | |
| Fatigue | 85 (85.8) | 11 (11.1) |
| Nausea | 76 (76.8) | 6 (6.1) |
| Diarrhea | 55 (55.5) | 3 (3.0) |
| Alopecia | 43 (43.4) | 0 (0) |
| Constipation | 30 (30.3) | 0 (0) |
| Pain | 22 (22.2) | 1 (1.0) |
| Vomiting | 19 (19.2) | 3 (3.0) |
| Anorexia | 19 (19.2) | 1 (1.0) |
| Cough | 15 (15.1) | 0 (0) |
| Abdominal pain | 15 (15.1) | 0 (0) |
| Neutrophil count decrease | 14 (14.1) | 12 (12.1) |
| Stomatitis | 10 (10.1) | 0 (0) |
| Anemia | 10 (10.1) | 0 (0) |

treatment by using imaging mass cytometry (IMC) and bulk RNA-seq to explore, first, the intratumoral distribution and the effects of HER3-DXd on TCs and its role in gene expression modulation and, second, the effects of HER3-DXd on the TME. By IMC, a multiple protein analytical method that relies on metal-tagged antibodies to simultaneously detect multiple proteins and provides spatial analysis, we detected the expression of 23 proteins (Supplementary Table 5 and Supplementary Fig. 10) at subcellular resolution (Hyperion) on FFPE tumor samples. We profiled 61 FFPE samples at BL and 57 on-treatement (on-T) (C1D3, C1D19 or C2D3), of which 39 were matched pairs. The heatmap of TC and immune cell density at baseline is shown in Supplementary Fig. 11. First, we explored the intracellular distribution of HER3-DXd in TCs and its association with treatment outcome, by using an anti-DXd antibody that selectively binds the DXd moiety linked to the antibody. The HER3-DXd expression was not found at BL, whereas a high proportion of both pan-keratin-positive ($PANK^+$) and pan-keratin-negative ($PANK^-$) cells were positive for intact-DXd in on-T tumor biopsies, with the highest values at C1D3 (Fig. 4a). We quantified $HER3\text{-}DXd^+$ cells across cell phenotypes ($PANK^+$, $PANK^-$, $PANK^+HER3^+$ and $PANK^+HER3^-$) at C1D3 and found a similar proportion of $HER3\text{-}DXd^+$ cells among $PANK^+$ (median: 10.4 (IQR 1.3–22.9)) and $PANK^-$ (median 10.2 (IQR 1.7–37.2)) cells, also with a comparable proportion of $HER3\text{-}DXd^+$ cells among the $PANK^+HER3^+$ (median 11.2 (IQR 0.9–26.5)) and the $PANK^+HER3^-$ (median 9.6 (IQR 1.3–24.6)) cells (Supplementary Table 6). Among the $HER3\text{-}DXd^+$ cells, the most prevalent phenotypes were $PANK^-$ and $PANK^+HER3^-$ (Extended Data Fig. 3a,b). Nevertheless, the interpretation of these data should take into account that the proportion of $HER3^+$ cells significantly reduced at C1D3 compared with BL (see below). As analyzable samples at C1D3 ($n = 20$) were all from patients who achieved CR, PR or SD, we then looked at the mean tumor shrinkage according to the proportion of $PANK^+HER3\text{-}DXd^+$ cells. We defined HER3-DXd positivity as having ≥5% positive cells. This threshold was chosen because, at BL (before any drug exposure), the maximum percentage of $HER3\text{-}DXd^+$ cells observed was 3.75%, likely due to background noise. Even with the limitation of the small sample size, we found that mean tumor shrinkage was −56.2% (s.d. = 23.4%) and −29.4% (s.d. = 20.4%) in patients with $PANK^+HER3\text{-}DXd^+$ cells ≥5% ($n = 11$) and $PANK^+HER3\text{-}DXd^+$ cells <5% ($n = 9$) at cycle 1 day 3 (Mann–Whitney *U*-test, $U = 17$, $P = 0.013$), respectively (Fig. 4b,c and Supplementary Fig. 12). Similarly, the mean tumor shrinkage was −55.0% (s.d. = 24.3%) and −33.3% (s.d. = 22.8%) in patients with $HER3\text{-}DXd^+$ cells above and below the median staining ($U = 25$, $P = 0.063$) (Supplementary Fig. 13). Although HER3-DXd positivity does not necessarily mean that an ADC has been internalized, we sought to evaluate whether the HER3-DXd positivity was associated with alterations or different expression of genes involved in the endocytosis pathway (*Clathrin*, *Dynamin2*, *Rab*, *Numb*, *Caveolin*, *LAMP1* and *CD71*). The genomic profile at BL was available for 7 of 11 patients with $HER3\text{-}DXd^+$ cells ≥5% ($HER3\text{-}DXd^+$ tumor) and 4 of 9 patients with $HER3\text{-}DXd^+$ cells <5% ($HER3\text{-}DXd^-$ tumor). We found that three of seven $HER3\text{-}DXd^+$ tumors harbored a genomic alteration in genes involved in endocytosis, of which one had a stop mutation in the *LAMP1* gene, one a synonymous mutation in *LAMP1* and one a synonymous mutation in *RAB11*, although we did not find any genomic alteration in these genes in the $HER3\text{-}DXd^-$ tumors. Transcriptomic profile at BL was available for 8 of 11 patients with $HER3\text{-}DXd^+$ tumors and 5 of 9 with $HER3\text{-}DXd^-$ ones. Differential expression analysis of RNA-seq data between the two groups did not reveal any significant difference of the expression of genes related to endocytosis (adjusted $P$ or $P_{adj} > 0.05$). As a specific tumor architecture potentially favoring the ADC intratumoral distribution (cluster 0) appeared to be linked to treatment response, we also analyzed the proportion of cluster 0 at BL in tumors with HER3-DXd positivity ≥5% and <5%, and did not find any statistically significant association (Supplementary Fig. 14).

Next, we characterized the dynamics of $HER3^+$ tumor cells after HER3-DXd administration and their association with response. We observed that HER3 expression dramatically decreased after HER3-DXd administration, with a greater decrease in responders (Student's *t*-test, $P = 0.011$; Extended Data Fig. 3c).

Then, to determine the effect of the ADCs on TCs, we analyzed on-T gene expression changes to identify which genes were modulated by HER3-DXd. We carried out bulk RNA-seq on 22 pairs of BL and on-T frozen tumor biopsies, collected 3 d or 19 d after cycle 1 or 3 d after cycle 2, selected to have tumor cellularity ≥30%. We conducted differential gene expression (DGE) analyses looking at the fold-change of gene expression of matched on-T BL samples in the overall population ($n = 22$) and, then, separately in responders (confirmed CR and PR; $n = 14$) and nonresponders (SD, PD and not evaluable; $n = 8$). A higher proportion of up- and downregulated genes was observed in responders ($n = 410$ genes) compared with nonresponders ($n = 5$ genes) after one or two doses of HER3-DXd ($P_{adj} \leq 0.05$; Fig. 4d,e). As most of the downregulated genes could be related to decreased cell proliferation, we further focused on upregulated genes to explore genes and pathways modulated by HER3-DXd. The top ten upregulated genes in responders were *EDA2R*, *IFI44L*, *RTP4*, *GBP1P1*, *IFIT1*, *IFIT2*, *AIM2*, *SELL*, *CLEC4E* and *IFIT3*, with $\log_2$(fold-change) between 0.88 and 0.68 ($P_{adj} \leq 0.05$). Most of these genes are involved in the interferon (IFN) signaling pathway. On consideration of the results of the IMC analysis showing an association between intratumoral detection of HER3-DXd and tumor shrinkage, we carried out DGE analyses of on-T samples of $HER3\text{-}DXd^+$ ($HER3\text{-}DXd^+$ cells ≥5%, $n = 5$) and $HER3\text{-}DXd^-$ tumors ($HER3\text{-}DXd^+$ cells <5%, $n = 7$). We observed a larger number of upregulated genes in $HER3\text{-}DXd^+$ compared with $HER3\text{-}DXd^-$ tumors ($P_{adj} \leq 0.05$; Fig. 4f). We further explored whether genes modulated by the drug administration clustered in specific pathways, by running

a GSEA. In the overall population, using the gene set Hallmarks, we observed an activation of pathways involved in immune response, particularly IFNα and IFNγ (gene ratio 0.45) and complement signaling (gene ratio 0.3; $P_{adj} \leq 0.05$; Extended Data Fig. 4a). Likewise, activation of pathways of immune response, notably IFNα and IFNγ, and complement signaling was found in responders ($P_{adj} \leq 0.05$; Extended Data Fig. 4b), whereas, in nonresponders, no gene set was modulated by treatment exposure ($P_{adj} > 0.05$). We also compared the pathways modulated on treatment between responders and nonresponders and confirmed that activation of immune-related pathways was enriched in responders compared with nonresponders ($P_{adj} \leq 0.05$; Extended Data Fig. 4c). However, we did not find any upregulation of IFN pathways in on-T HER3-DXd$^+$ compared with HER3-DXd$^-$ tumors (Extended Data Fig. 4d). Finally, among the 54 Kyoto Encyclopedia of Genes and Genomes (KEGG) gene sets modulated by the treatment, we could identify that the 'endocytosis' gene set was suppressed on treatment (gene ratio 0.36; $P_{adj} \leq 0.05$), a finding possibly related to an adaptation of cancer cells to therapy (Supplementary Fig. 15). We also performed GSEA using the gene set Hallmarks according to CBR and, consistent with the previous results, we found activation of immune-related pathways in patients with CBR ($n = 16$) compared with those without (n = 6; $P_{adj} \leq 0.05$; Supplementary Fig. 16).

Given the IFN response observed in sensitive patients, we evaluated PFS in patients with upregulation of the IFNα or IFNγ pathway versus those presenting a stable or downregulated pathway. We observed a trend toward a longer PFS in patients with either α ($P = 0.26$) or γ ($P = 0.04$) pathway activation (Extended Data Fig. 5).

As the second step in determining the mechanism of action of T-DXd, we evaluated its impact on the TME. To this end, we investigated how HER3-DXd modulated the immune cell composition in the tumor and TME. Despite the activation of IFNα and IFNγ pathways being associated with a better treatment outcome (ORR, CBR or PFS), we found both increases and decreases of T cells with no clear differences between responders and nonresponders. However, the most significant increase in CD3$^+$CD4$^+$, CD3$^+$CD8$^+$ and CD3$^+$CD8$^+$CD107a$^+$ cell densities was seen in two responders, whereas the greatest increase in CD3$^+$CD8$^+$GzmB$^+$ cell density occurred in one of these two patients (Extended Data Fig. 6a–d and Supplementary Table 7). We also observed that CD68$^+$ cell density was decreased in the TME after one or two doses of HER3-DXd, without any difference between responders and nonresponders (Extended Data Fig. 6e). We finally performed immune deconvolution analysis using CIBERSORTx_ABSOLUTE on paired on-T versus BL tumor samples ($n = 22$) to assess changes in immune cell subpopulations. However, we did not observe any significant increase or decrease in specific immune cell subsets in responders ($n = 14$) compared with nonresponders ($n = 8$), suggesting that HER3-DXd did not induce major shifts in the immune composition of the TME (Supplementary Fig. 17).

## Discussion

In the ICARUS-BREAST01 study, HER3-DXd showed considerable efficacy in patients with HR$^+$HER2$^-$ advanced breast cancer who had previously progressed on CDK4/6 inhibitors and one line of chemotherapy. Most of the patients achieved a confirmed treatment response (ORR 53.5%) and experienced prolonged disease control. In addition, HER3-DXd showed a manageable safety profile, with a low rate of grade ≥3 TRAEs and TRAEs leading to treatment discontinuation. Notably, the rate of ILD adjudicated as drug related was low (8.1%), most being grade 1 and thus allowing treatment recovery at ILD resolution, except in three cases. T-DXd was approved by the US Food and Drug Administration for patients with inoperable or metastatic HR$^+$HER2-low breast cancer after at least one line of chemotherapy and, more recently, also for patients with HR$^+$HER2-low or HER2-ultralow breast cancer that has progressed after at least one endocrine therapy in the metastatic setting, based on the remarkable results of the DESTINY-Breast04 and DESTINY-Breast06 trials[10,25]. Overall, the clinical results of the ICARUS-BREAST01 study appear to be comparable to those observed with T-DXd in the DESTINY-Breast04 study, although the latest included a more pretreated population[10]. For these patients, T-DXd is not an option if HER2 expression is <1% (about 20% of HER2-nonoverexpressing tumors)[25,26] and the efficacy of T-DXd in the HER2-ultralow setting was based on exploratory analyses of the DESTINY-Breast06 study. Therefore, the ICARUS-BREAST01 findings emphasize the need for a large phase 3 study in patients with HR$^+$HER2$^-$ breast cancer, who can no longer benefit from endocrine therapy, to determine the efficacy of HER3-DXd in HER2-null tumors and also in HER2-low or HER2-ultralow breast cancers, in which it could be a valuable alternative to T-DXd, considering some differences in the safety profile. This study would also provide an opportunity to further validate the preliminary findings, suggesting a positive trend between HER3-enriched populations and PFS, which helps to refine patient selection strategies. Furthermore, although the ICARUS-BREAST01 study excluded patients previously treated with ADCs, because they were designed before the results of the pivotal trials of DESTINY-Breast04, TROPICS-02 and DESTINY-Breast06 (refs. 10,12,25), we recognize the importance of investigating the activity of HER3-DXd after previous ADCs. Previous clinical data showed that ADC resistance may sometimes derive from reduced target expression, while preserving payload sensitivity[27–29]. Leveraging these preclinical and clinical data, we designed the ICARUS-BREAST02 study (NCT06298084), which is currently evaluating the efficacy and tolerability of HER-DXd either as a single agent or in combination with olaparib in patients who have progressed on previous treatment with T-DXd.

An essential part of our study was to explore biomarkers of response to HER3-DXd by analyzing tumor samples at BL and understand mechanisms of action of the drug, by analyzing the effect of HER3-DXd on the tumor and the TME of samples collected on-T. To identify potential predictors of response, we first explored the role of the target expression and spatial distribution in predicting treatment outcome. Although there was no association between ORR and HER3 expression, we found a trend toward a longer PFS in patients with higher HER3 expression. This trend was consistently observed across all three scoring methods. Therefore, although this association did not reach statistical significance, potentially due to the small sample size, and does not allow for the definition of a clear HER3 expression threshold,

**Fig. 3 | HER3 expression and spatial mapping at BL and association with treatment response. a**, Box plot showing the proportion of HER3 1+, 2+ and 3+ TCs at BL and best overall treatment response. **b**, Kaplan–Meier estimates of PFS according to HER3-membrane 2+ and 3+ ≥50% of TCs (left) and according to HER3-membrane 1+, 2+ and 3+ in ≥75% of TCs (right) (for both $n = 72$ and no. of events = 46). **c**, Clusters of HER3 or neighborhood cell distribution. Digitized DAB-stained slides were overlapped with digitized H&E-stained slides. These regions were then segmented into eight different clusters. Box plots show the proportion of each cluster in 63 evaluable patients, according to treatment response: responders (CR, PR) and nonresponders (SD, PD). The box center lines, box ranges, whiskers and dots indicate the medians, quartiles, 1.5× the IQR and outliers, respectively. Our analysis revealed an association between treatment response and the percentage of cluster 0 ($P = 0.040$), with an odds ratio of 1.527 95% CI [1.020–2.287]. For all these analyses, using R v.4.1.2, we applied Dirichlet's regression to identify which clusters were significantly associated with the objective response to treatment (statistical significance was assessed using Wald's test based on Dirichlet-distributed parameters; the reported $P$ values were unadjusted for multiple comparisons). **d**, H&E-stained slide showing the composition of cluster 0, characterized by a moderate number of TCs, surrounded by connective areas, with a few immune cells and no necrotic areas. **e**, Proportion of the different cell phenotypes (epithelial, connective, inflammatory, necrotic and neoplastic areas) across the identified clusters ($n = 63$). The box center lines, box ranges, whiskers and dots indicate the medians, quartiles, 1.5× the IQR and outliers, respectively.

https://doi.org/10.1038/s41591-025-03885-3

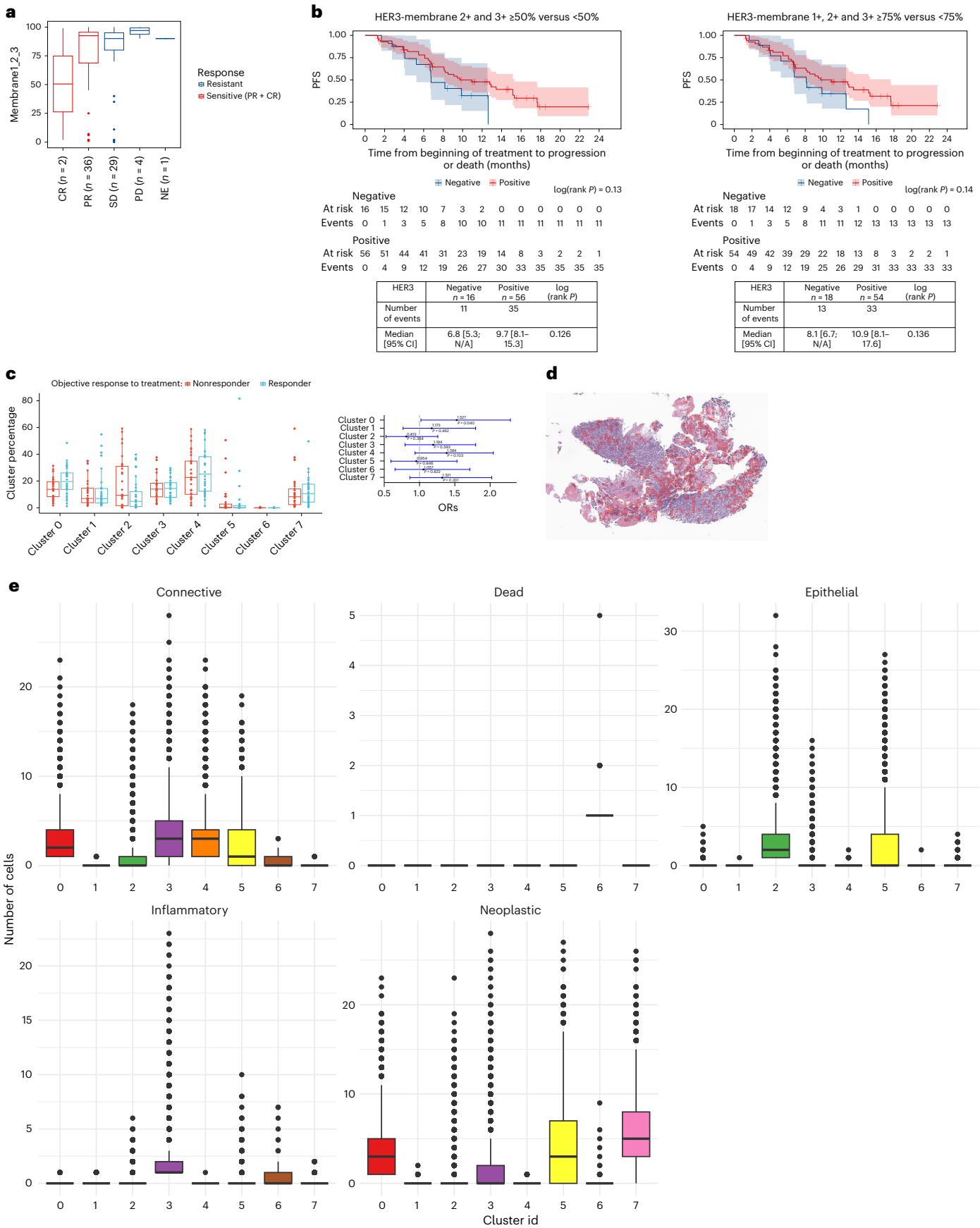

https://doi.org/10.1038/s41591-025-03885-3

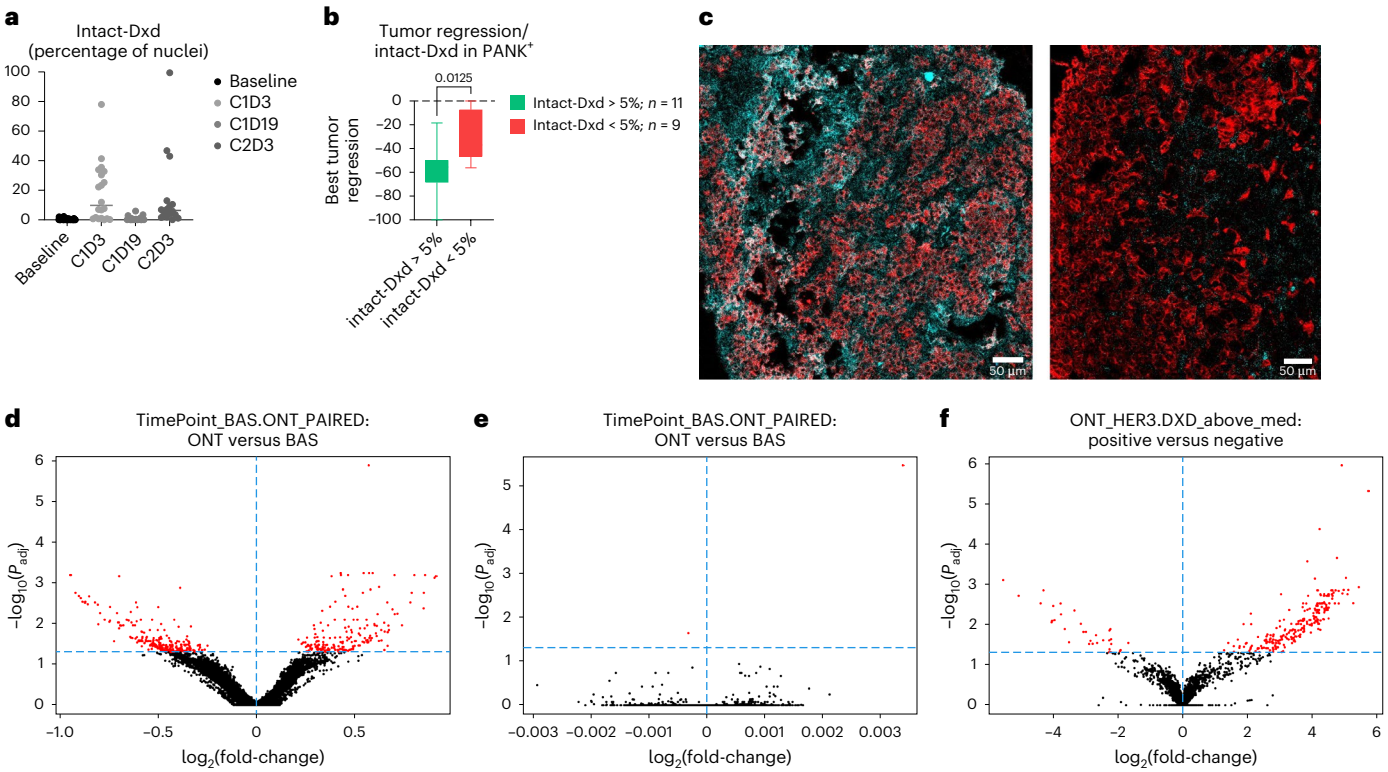


**Fig. 4 | HER3-DXd intratumoral distribution and interaction with TCs.** **a**, Dynamics of HER3-DXd$^+$ cells over the different time points. **b**, Mean tumor shrinkage in patients with ≥5% of HER3-DXd$^+$ cells and those with <5% HER3-DXd$^+$ cells at C1D3 (Student's *t*-test, $P = 0.0146$). The 5% cut-off was chosen according to the minimal detectable percentage of HER3-DXd$^+$ cells. The boxes represent the IQR and the whiskers extend to the minimum and maximum values within each group. **c**, Left: image of a tumor with HER3-DXd staining ≥5% of TCs at C1D3: intact-DXd$^+$ cells 21% of the PANK$^+$ cells. Right: image of a tumor with HER3-DXd staining <5% of TCs at C1D3: intact-DXd$^+$ cells 0.25% of the PANK$^+$ cells. PANK$^+$ cells are shown in red and Intact-DXd$^+$ cells in blue; similar staining patterns were observed across all analyzed samples ($n = 20$). **d**,**e**, Volcano plot of differentially expressed genes in paired on-T and BL tumor samples in responders (**d**) and nonresponders (**e**). The *P* values shown are from two-sided tests and were adjusted for multiple comparisons using the Benjamini–Hochberg method. **f**, Volcano plot of differentially expressed genes in on-treatment samples of HER3-DXd$^+$ (≥5% TCs, $n = 5$) and HER3-DXd$^-$ (<5% TCs, $n = 7$) tumors. The *P* values shown are from two-sided tests and were adjusted for multiple comparisons using the Benjamini–Hochberg method.

it remains a promising finding that warrants further investigation. It is interesting that we did not find a strong association between HER2 and HER3 expression, because there are tumors with high HER3 expression that have HER2-0 or HER2-low expression, reinforcing the interest in further determining the efficacy of HER3-DXd in both settings. Furthermore, using machine learning analysis on IHC and H&E slides, we found that the distribution of HER3$^+$ TCs within tumor tissue may play a role in determining a better ADC penetration and distribution. Indeed, tumors with a higher proportion of cluster 0, and thus containing a moderate number of HER3$^+$ cells and being surrounded by connective tissue areas and no necrotic areas, had a higher likelihood of responding to the treatment. It is important to note that the association between cluster 0 and treatment outcome may not be driven solely by the spatial distribution of HER3$^+$ cells relative to neighboring cells. Instead, it could be the result of a specific tumor architecture favoring the ADC intratumoral distribution, independent of HER3 expression. Indeed, when HER3 staining was excluded from the clustering algorithm, two response-associated clusters were identified, of which one (1*) shared features with cluster 0, including TCs surrounded by connective tissue, sparse immune cells and absence of necrotic areas, and the other (0*) containing only connective tissue, interpreted as not biologically relevant. The composition of the 0* clusters and lack of significance of similar clusters in the initial analysis led us to interpret it as a compositional artifact, in contrast to clusters 0 and 1* sharing similar biological characteristics with a more straightforward interpretation. As Dirichlet-regression models have relative, rather than absolute, cluster proportions, significant clusters can also emerge due to shifts in other clusters, not necessarily reflecting direct association with treatment response. Given the limited sample size and novelty of the mechanisms, these analyses remain nevertheless exploratory and hypothesis generating, requiring validation in independent cohorts to confirm the relevance of HER3 spatial mapping.

We also investigated whether driver mutations in breast cancer and genomic alterations of interest in DXd activity (for example, *TOP1mut*) could be associated with the response to treatment. We did not find any association between response to HER3-DXd and known breast cancer driver mutations or alterations in genes involved in HER3-DXd activity, except for *ERBB3mut* which was more frequent in responders (11.5%) versus nonresponders (5.9%). Although most *ERBB3mut* changes occur in the extracellular domain, previous preclinical data did not show differences in HER3-DXd activity across cell lines with or without *ERBB3mut*[30]. Furthermore, we observed that tumors harboring *ESR1mut* were more likely to be resistant to HER3-DXd (52.9% in nonresponders and 23.1% in responders). Although *ESR1mut* tumors are resistant to aromatase inhibitors and tend to be more heavily pretreated, we did not find any significant difference in the clinical characteristics of patients with *ESR1mut* tumors and those with *ESR1wt* tumors, such as the number of previous systemic therapies and time from initial diagnosis to study entry. Likewise, the median number of genomic alterations along with tumor mutational burden were similar in the two groups. However, given the small sample size, these data should be interpreted with caution. Previous preclinical studies demonstrated a bidirectional crosstalk between the ER signaling pathway and the HER3 or HER2 pathway in ER$^+$ breast cancer[31]. For instance, it has

been shown that exposure to tamoxifen or fulvestrant, which inhibits ER signaling, also increases epidermal growth factor receptor, HER2 and HER3 expression[32,33]. Therefore, it is possible that, in *ESR1mut* tumors, the constitutive activation of the ER pathway, as we found in our cohort, can be associated with downregulation of HER3. Furthermore, although no differences in the PAM50-subtype assignment were observed between *ESR1mut* and *ESR1wt* tumors in our cohort, it is likely that *ESR1mut* tumors exhibit more luminal characteristics which may reduce the response to HER3-DXd. This aligns with the observed higher prevalence of *TP53* mutations in responders and previous clinical findings, because these mutations are associated with more proliferative and chemosensitive tumor profiles[34].

The exploratory analysis of the ICARUS-BREAST01 study also aimed to decipher the key mechanisms of action of HER3-DXd and particularly its interaction with the tumor and the TME. With this objective, we analyzed on-treatment tumor samples by IMC and bulk RNA-seq. IMC analysis revealed that tumors with a higher proportion of PANK$^+$HER3-DXd$^+$ cells 3 d after cycle 1 had a deeper treatment response. Although HER3-DXd$^+$ cells at IMC do not necessarily indicate that the ADC has been internalized, we can hypothesize that a greater ability of ADCs to penetrate tumor tissues could allow a higher ADC uptake by TCs and ultimately increase cell death. DGE analysis further supported these findings, showing a greater number of modulated genes in responders compared with nonresponders and also in HER3-DXd$^+$ tumors compared with HER3-DXd$^-$ ones. Although the DGE modulation cannot exclude a resistance to the payload, these data suggest that an impaired HER3-DXd tumor penetration may significantly limit the proportion of the DXd interacting with tumor cells. These preliminary findings raise the hypothesis that the ADC tumor penetration and cell internalization may play a critical role in determining ADC efficacy. Furthermore, these results induce consideration of new strategies for early detection of ADC uptake in TCs and prediction of treatment response. For example, new technologies for the detection of ADC uptake in circulating tumor cells (CTCs) could represent a significant advancement in monitoring ADC efficacy in real-time.

Furthermore, gene expression analysis of matched on-T or BL samples showed upregulation of genes involved in immune response, particularly IFNα and IFNγ, and complement signaling significantly enriched in the entire cohort, in particular among responders. It is possible that DXd-induced DNA damage activates the cGAS–cGAMP–STING pathway, leading to the upregulation of type I IFNs in tumor cells, which has been associated with better treatment outcomes (ORR and PFS). These findings suggest that a greater ADC intratumoral distribution can lead to a greater ADC intracellular uptake and DNA damage, resulting in an IFN response in tumor cells[35,36]. However, in our study, the exploration of immune TME composition by IMC on paired tumor samples at BL and on-T showed a notable T cell expansion and activation (increase of CD4$^+$, CD8$^+$, CD8$^+$GzmB$^+$ and CD8$^+$CD107a$^+$) after 3 d from cycle 1 in only two patients who achieved tumor response to the treatment. Similarly, immune deconvolution analysis did not show any significant upregulation of immune cells. Although IFNα and IFNγ activation in tumors may indicate a response to treatment, the absence of immune cell expansion is likely driven by the immunosuppressive nature of the TME and also by additional contributing factors, such as the low density of immune cells at BL (as shown in Supplementary Table 9 and Supplementary Fig. 11), likely related to the predominance of liver metastases in the biopsy samples, known for their inherently low immune infiltration, and the possibility that the on-T time point was not optimal for capturing the immune cell expansion that is likely to happen later on. Therefore, it would be worthwhile exploring, in the future, IFNα and IFNγ activation in CTC, as an early predictor of optimal drug–tumor interactions and, ultimately, treatment response, so helping to refine patient selection and treatment strategies.

Our study has several limitations that should be acknowledged. First, the sample size was relatively small and the study was a nonrandomized single-arm trial, which lacks the rigor of randomized controlled trials, and treatment response has not been confirmed by a blinded independent central review. Nevertheless, the high efficacy of HER3-DXd demonstrated in the ICARUS-BREAST01 study, also confirmed by the central review, certainly warrants being confirmed in larger trials in similar settings. Second, we included a higher proportion of patients with HER2-0 breast cancer than we would have expected[37], which was due to the almost simultaneous activation of an expanded access program for T-DXd in HER2-low breast cancer in France (https://www.has-sante.fr/jcms/p_3341817/fr/enhertu-trastuzumab-deruxtecan-cancer-du-sein-her2), which limited the inclusion of these patients. Although these patients' characteristics could affect the generalizability of the clinical results, we did not find significant differences in treatment outcome between patients with HER2-0 and those with HER2-low breast cancer. In addition, the limited sample size, the lack of information on tumor biology at study entry (for example, ER expression) and the absence of a validation cohort for several of the translational findings may affect the robustness and reproducibility of the biomarker analyses. However, the high proportion of tumor samples collected at BL and on-T in this study offers a unique opportunity for generating a hypothesis on some of the key mechanisms of response and resistance to HER3-DXd.

In conclusion, the ICARUS-BREAST01 study shows a substantial efficacy and a manageable safety profile of HER3-DXd in patients with HR$^+$HER2$^-$ breast cancer that make it an optimal candidate for further larger studies in this setting. This study also identifies potential biomarkers of treatment response and provides some insights into the mechanisms of action of HER3-DXd. Although limited by the nature of purely exploratory analyses, our findings generate a hypothesis on the mechanism of action of this ADC, suggesting that target expression and spatial distribution, and ADC intratumoral distribution, intracellular uptake and subsequent DNA damage, may influence treatment response. These findings warrant further investigations and underline the importance of further studies, employing similar approaches, to define biomarkers that will allow optimal patient selection for a given ADC. Despite the challenges associated with serial sample collection and analysis, such studies are nevertheless important in providing a comprehensive understanding of the mechanisms of action of new ADCs.

## Online content

Any methods, additional references, Nature Portfolio reporting summaries, source data, extended data, supplementary information, acknowledgements, peer review information; details of author contributions and competing interests; and statements of data and code availability are available at https://doi.org/10.1038/s41591-025-03885-3.

## References

1. Siegel, R. L., Giaquinto, A. N. & Jemal, A. Cancer statistics, 2024. *CA Cancer J. Clin.* **74**, 12–49 (2024).
2. Sedeta, E. T., Jobre, B. & Avezbakiyev, B. Breast cancer: global patterns of incidence, mortality, and trends. *J. Clin. Oncol.* **41**, 10528–10528 (2023).
3. Drago, J. Z., Modi, S. & Chandarlapaty, S. Unlocking the potential of antibody–drug conjugates for cancer therapy. *Nat. Rev. Clin. Oncol.* **18**, 327–344 (2021).
4. Mosele, F., Montagnac, G., Pistilli, B. & André, F. Optimizing the potential of antibody–drug conjugates in oncology. *Ann. Oncol.* **34**, 964–967 (2023).
5. Coates, J. T. et al. Parallel genomic alterations of antigen and payload targets mediate polyclonal acquired clinical resistance to sacituzumab govitecan in triple-negative breast cancer. *Cancer Discov.* **11**, 2436–2445 (2021).
6. Peters, C. & Brown, S. Antibody–drug conjugates as novel anti-cancer chemotherapeutics. *Biosci. Rep.* **35**, e00225 (2015).

7. Tarcsa, E., Guffroy, M. R., Falahatpisheh, H., Phipps, C. & Kalvass, J. C. Antibody-drug conjugates as targeted therapies: are we there yet? A critical review of the current clinical landscape. *Drug Discov. Today Technol.* **37**, 13–22 (2020).
8. Hoogenboezem, E. N. & Duvall, C. L. Harnessing albumin as a carrier for cancer therapies. *Adv. Drug Deliv. Rev.* **130**, 73–89 (2018).
9. Colombo, R., Tarantino, P., Rich, J. R., LoRusso, P. M. & De Vries, E. G. E. The journey of antibody–drug conjugates: lessons learned from 40 years of development. *Cancer Discov.* **14**, 2089–2108 (2024).
10. Modi, S. et al. Trastuzumab deruxtecan in previously treated HER2-low advanced breast cancer. *N. Engl. J. Med.* **387**, 9–20 (2022).
11. André, F. et al. Trastuzumab deruxtecan versus treatment of physician's choice in patients with HER2-positive metastatic breast cancer (DESTINY-Breast02): a randomised, open-label, multicentre, phase 3 trial. *Lancet* **401**, 1773–1785 (2023).
12. Rugo, H. S. et al. Overall survival with sacituzumab govitecan in hormone receptor-positive and human epidermal growth factor receptor 2-negative metastatic breast cancer (TROPiCS-02): a randomised, open-label, multicentre, phase 3 trial. *Lancet* **402**, 1423–1433 (2023).
13. Bardia, A. et al. Datopotamab deruxtecan versus chemotherapy in previously treated inoperable/metastatic hormone receptor-positive human epidermal growth factor receptor 2-negative breast cancer: primary results from TROPION-Breast01. *J. Clin. Oncol.* **43**, 285–296 (2025).
14. Mosele, F. et al. Trastuzumab deruxtecan in metastatic breast cancer with variable HER2 expression: the phase 2 DAISY trial. *Nat. Med.* **29**, 2110–2120 (2023).
15. Pistilli, B. et al. 189O A phase II study of patritumab deruxtecan (HER3-DXd), in patients (pts) with advanced breast cancer (ABC), with biomarker analysis to characterize response to therapy (ICARUS-BREAST01). *ESMO Open* **8**, 101378 (2023).
16. Gennari, A. et al. ESMO Clinical Practice Guideline for the diagnosis, staging and treatment of patients with metastatic breast cancer. *Ann. Oncol.* **32**, 1475–1495 (2021).
17. Moy, B., Rumble, R. B., Carey, L. A. & Metastatic Breast Cancer Expert Panel. Chemotherapy and targeted therapy for endocrine-pretreated or hormone receptor-negative metastatic breast cancer: ASCO Guideline rapid recommendation update. *J. Clin. Oncol.* **41**, 1318–1320 (2023).
18. Turner, N. C. et al. Capivasertib in hormone receptor-positive advanced breast cancer. *N. Engl. J. Med.* **388**, 2058–2070 (2023).
19. Kalinsky, K. et al. Randomized phase II trial of endocrine therapy with or without ribociclib after progression on cyclin-dependent kinase 4/6 inhibition in hormone receptor-positive, human epidermal growth factor receptor 2-negative metastatic breast cancer: MAINTAIN trial. *J. Clin. Oncol.* **41**, 4004–4013 (2023).
20. Hortobagyi, G. N. et al. Updated results from MONALEESA-2, a phase III trial of first-line ribociclib plus letrozole versus placebo plus letrozole in hormone receptor-positive, HER2-negative advanced breast cancer. *Ann. Oncol.* **29**, 1541–1547 (2018).
21. Im, S.-A. et al. Overall survival with ribociclib plus endocrine therapy in breast cancer. *N. Engl. J. Med.* **381**, 307–316 (2019).
22. Papa, F. et al. Long road towards effective HER3 targeting in breast cancer. *Cancer Treat. Rev.* **129**, 102786 (2024).
23. Krop, I. E. et al. Patritumab deruxtecan (HER3-DXd), a human epidermal growth factor receptor 3-directed antibody–drug conjugate, in patients with previously treated human epidermal growth factor receptor 3-expressing metastatic breast cancer: a multicenter, phase I/II trial. *J. Clin. Oncol.* **41**, 5550–5560 (2023).
24. Van Der Sluijs, P. et al. The small GTP-binding protein rab4 controls an early sorting event on the endocytic pathway. *Cell* **70**, 729–740 (1992).
25. Bardia A. et al. Trastuzumab deruxtecan after endocrine therapy in metastatic breast cancer. *N. Engl. J. Med.* **391**, 2110–2122 (2024).
26. Curigliano, G. et al. Trastuzumab deruxtecan (T-DXd) vs physician's choice of chemotherapy (TPC) in patients (pts) with hormone receptor-positive (HR+), human epidermal growth factor receptor 2 (HER2)-low or HER2-ultralow metastatic breast cancer (mBC) with prior endocrine therapy (ET): primary results from DESTINY-Breast06 (DB-06). *J. Clin. Oncol.* **42**, LBA1000 (2024).
27. Bardia, A. et al. Datopotamab deruxtecan in advanced or metastatic $HR^{+}/HER2^{-}$ and triple-negative breast cancer: results from the phase I TROPION-PanTumor01 study. *J. Clin. Oncol.* **42**, 2281–2294 (2024).
28. Abelman, R. O. et al. Sequential use of antibody-drug conjugate after antibody-drug conjugate for patients with metastatic breast cancer: ADC after ADC (A3) study. *J. Clin. Oncol.* **41**, 1022 (2023).
29. Huppert, L. et al. Multicenter retrospective cohort study of the sequential use of the antibody-drug conjugates (ADCs) trastuzumab deruxtecan (T-DXd) and sacituzumab govitecan (SG) in patients with HER2-low metastatic breast cancer (MBC). *Cancer Res.* **84**, abstr. PS08-04 (2024).
30. Koyama, K. et al. Patritumab deruxtecan (HER3-DXd), a novel HER3 directed antibody drug conjugate, exhibits in vitro activity against breast cancer cells expressing HER3 mutations with and without HER2 overexpression. *PLoS ONE* **17**, e0267027 (2022).
31. Thrane, S., Lykkesfeldt, A. E., Larsen, M. S., Sorensen, B. S. & Yde, C. W. Estrogen receptor α is the major driving factor for growth in tamoxifen-resistant breast cancer and supported by HER/ERK signaling. *Breast Cancer Res. Treat.* **139**, 71–80 (2013).
32. Hutcheson, I. R. et al. Fulvestrant-induced expression of ErbB3 and ErbB4 receptors sensitizes oestrogen receptor-positive breast cancer cells to heregulin β1. *Breast Cancer Res.* **13**, R29 (2011).
33. Liu, B. et al. Downregulation of erbB3 abrogates erbB2-mediated tamoxifen resistance in breast cancer cells. *Int. J. Cancer* **120**, 1874–1882 (2007).
34. Brasó-Maristany, F. et al. Patritumab deruxtecan in HER2-negative breast cancer: part B results of the window-of-opportunity SOLTI-1805 TOT-HER3 trial and biological determinants of early response. *Nat. Commun.* **15**, 5826 (2024).
35. Samson, N. & Ablasser, A. The cGAS–STING pathway and cancer. *Nat. Cancer* **3**, 1452–1463 (2022).
36. Oh, K.-S. et al. Immunomodulatory effects of trastuzumab deruxtecan through the cGAS-STING pathway in gastric cancer cells. *Cell Commun. Signal.* **22**, 518 (2024).
37. Tarantino, P. et al. HER2-low breast cancer: pathological and clinical landscape. *J. Clin. Oncol.* **38**, 1951–1962 (2020).

https://doi.org/10.1038/s41591-025-03885-3

**Barbara Pistilli[1,2,3] ✉, Fernanda Mosele[1,3,4,26], Noemie Corcos[2,3,26], Livia Pierotti[3,5], Yoann Pradat[3,4], Loic Le Bescond[3,4,6], Magali Lacroix-Triki[3,7], Ghada Nachabeh[8], Alexia Alfaro[9], Cyril Catelain[9], Bastien Job[3,4], Fathia Mami-Chouaib[10], Severine Badel[10], Françoise Farace[3,4,11], Marianne Oulhen[3,4,11], Patricia Kannouche[12], Diep T. N. Tran[3,4], Nathalie Droin[3,9], Cecile Vicier[13], Jean Sebastien Frenel[14,15], Veronique D'Hondt[16], Florence Dalenc[17], Thomas Bachelot[18], Agnes Ducoulombier[19], Marc Antoine Benderra[20], Delphine Loirat[21], Didier Mayeur[22], Elise Deluche[23], Jacqueline Deneuve[1], Rasha Cheikh-Hussin[2], Pierre Guyader[5], Nicolas Signolle[7], Karine Godefroy[7], Hugues Talbot[6], Maria Vakalopoulou[3,6], Stergios Christodoulidis[3,24], Elsa Bernard[3,4], Yves Koudou[5], Andrea Sporchia[25], Fumitaka Suto[25], Lie Li[25], David W. Sternberg[25], Stefan Michiels[3,5], Fabrice André[1,3,4], Dalila Sellami[25] & Guillaume Montagnac[2,3]**

[1]Department of Medical Oncology, Gustave Roussy, Villejuif, France. [2]INSERM 1279, Gustave Roussy, Villejuif, France. [3]IHU PRISM National PRecISion Medicine Center in Oncology, Gustave Roussy, Villejuif, France. [4]INSERM U981, Gustave Roussy, Paris, France. [5]Office of Biostatistics and Epidemiology, Gustave Roussy, Oncostat INSERM U1018, Université Paris-Saclay, Ligue Contre le Cancer, Villejuif, France. [6]CentraleSupélec, Inria, Université Paris-Saclay, Gif-Sur-Yvette, France. [7]Department of Pathology, Gustave Roussy, Villejuif, France. [8]Projects and Promotion Division, Gustave Roussy, Villejuif, France. [9]UMS AMMICa, CNRS UAR 3655, INSERM US23, Gustave Roussy, Villejuif, France. [10]UMR1186, Gustave Roussy, Villejuif, France. [11]Gustave Roussy, Université Paris-Saclay, 'Rare Circulating Cells' Translational Platform, CNRS UMS3655 – INSERM US23 AMMICA, Villejuif, France. [12]UMR9019-CNRS, Université Paris-Saclay, Gustave Roussy, Villejuif, France. [13]Department of Medical Oncology, Institut Paoli Calmettes, Marseille, France. [14]Department of Medical Oncology, Institut de Cancerologie de l'Ouest, Saint Herblain, France. [15]Nantes Université, INSERM, Centre de Recherche en Cancérologie et Immunologie Nantes Angers, Nantes, France. [16]Department of Medical Oncology, Institut Régional du Cancer de Montpellier, Montpellier, France. [17]Department of Medical Oncology, Oncopole Claudius Regaud, Toulouse, France. [18]Department of Medical Oncology, Centre Léon Bérard, Lyon, France. [19]Department of Medical Oncology, Centre Antoine Lacassagne, Nice, France. [20]Department of Medical Oncology, Tenon Hospital, APHP, Paris, France. [21]Department of Medical Oncology, Curie Hospital, Paris, France. [22]Department of Medical Oncology, Centre Georges François Leclerc, Dijon, France. [23]Department of Medical Oncology, Centre Hopital-Universitaire, Limoges, France. [24]CentraleSupélec, Université Paris-Saclay, Gif-Sur-Yvette, France. [25]Daiichi Sankyo Inc., Basking Ridge, NJ, USA. [26]These authors contributed equally: Fernanda Mosele, Noemie Corcos.
✉e-mail: barbara.pistilli@gustaveroussy.fr

## Methods

### Study design and sample collection

The ICARUS-BREAST01 study (NCT04965766) is an academic, single-arm, phase 2 study which has been conducted across 11 cancer centers or hospitals in France. The following are the key eligibility criteria: female or male patient aged ≥18 years; locally advanced or metastatic (MBC) that was $HR^+$ ($ER^+$ and/or $PR^+$) and $HER2^-$ (IHC 2+ and ISH negative, or IHC 1+ or IHC 0+) at the time of the first diagnosis (if the tumor were $ER^+$ and/or $PR^+$ at initial diagnosis and became $ER^-$ and/or $PR^-$ in the following biopsies performed while receiving previous standard treatments for MBC, the patient could be included); progression on endocrine therapy and CDK4/6 inhibitors; must have received one line, but not more than one, of chemotherapy for MBC; may have received previous treatment with PI3K inhibitors, mTOR inhibitors, AKT inhibitors and poly(ADP) ribose polymerase inhibitors; must have metastatic site easily accessible to biopsy (with the exception of bone metastasis) and have accepted the performance of pre-treatment and on-treatment biopsies; and Eastern Cooperative Oncology Group performance status 0 or 1.

The study was initially designed to include only patients with HER3 membrane expression ≥75% with 10× in-tumor biopsies at BL; however, this inclusion criterion was deleted by amendment on 21 April 2022, after inclusion of the first 29 patients; afterwards recruitment proceeded regardless of HER3 expression. This decision was taken because data across different tumor types, including breast cancer, showed HER3-DXd clinical benefit across a broad range of tumor HER3 expression levels[23]. Patients with clinically inactive or treated brain metastases who were asymptomatic were eligible, whereas patients with any history of ILD (including pulmonary fibrosis or radiation pneumonitis), current confirmed or suspected ILD or with clinically severe intercurrent pulmonary illnesses or previous treatment with an ADC containing a topoisomerase-I inhibitor payload were excluded. Mandatory tumor biopsies were performed (1 frozen + 3 FFPE): pre-treatment (baseline), on-T and at the end of treatment. For on-T tumor biopsies, patients were divided into three groups to undergo a single on-T biopsy at the following time points: group 1 (34% of patients) at C1D3 ± 1 d, group 2 (33% of patients) at C1D19 ± 1 d and group 3 (33% of patients) at C2D3 ± 1 d (1 frozen + 3 FFPE). Serum and blood samples were also collected at multiple time points, which are detailed in the first and last versions of the protocol provided in Supplementary Information. Patients received treatment with HER3-DXd 5.6 mg $kg^{-1}$ every 3 weeks until investigator-assessed radiological progression (per RECIST v.1.1), unacceptable toxicity, withdrawal of consent or any other discontinuation criterion indicated in the protocol. The protocol was submitted to the competent ethics committee (CPP), which gave its approval on 12 March 2021. This study was also approved by the competent authority on 29 April 2021 and performed in accordance with the ethical principles of the Declaration of Helsinki and consistent with the International Conference on Harmonisation Good Clinical Practice guidelines and other applicable regulatory requirements. All patients provided written informed consent before study participation.

### Statistical analysis

The primary statistical test was a one-sided exact test for a binomial proportion. The null hypothesis was that the treatment with HER3-DXd yields an ORR ≤ 12%; 99 patients were required to provide 85% power to test this null hypothesis at a one-sided 5% significance level, assuming an ORR of 23% under the alternative hypothesis. The primary endpoint, ORR, was defined as the proportion of patients who achieved a confirmed CR or PR, as assessed by local investigators, without initiation of new anticancer treatment. Confirmation of response had to be demonstrated with an assessment 4 weeks or later after the initial response. The treatment objective response was radiologically assessed every 6 weeks using RECIST v.1.1. For equivocal findings of progression (for example, very small and uncertain new lesions, cystic changes or necrosis in existing lesions), treatment was allowed until the next scheduled assessment. Tumor imaging assessment was performed every 6 weeks (±7 d) starting at 6 weeks from the first dose for the first 12 months and then every 12 weeks (±7 d). Secondary endpoints were: PFS by investigator assessment, DoR, CBR, OS and safety. CBR was defined as the presence of at least a PR or CR, or a SD for ≥6 months under treatment.

The 95% CIs for rates such as ORR and CBR were calculated using the Clopper–Pearson method. A waterfall plot was also used to present each patient's (unconfirmed or confirmed) ORR according to their variation for the minimum sum of the patient's tumor size from baseline.

Kaplan–Meier estimations and curves were used to describe DoR, PFS and OS. PFS was defined as the time from the date of the first dose until documented disease progression or death from any cause, whichever occured first. For patients with no documented radiological progression, follow-up was censored at the date of last radiological assessment without progression, unless death occurred within 12 weeks of the date of last known progression free, in which case the death was counted as a PFS event. The DoR was calculated for the patients with either confirmed CR or PR and defined as the time from the first documented confirmed CR or PR until the date of disease progression or the date of death. Follow-up time was calculated using the reverse Kaplan–Meier method[38]. Safety endpoints (AEs, AESIs, serious adverse events (SAEs), TEAEs and TRAEs), defined by the National Cancer Institute Common Terminology Criteria for Adverse Events v.5.0 (NCI-CTCAE v.5.0) were described as maximum grade for each patient by the CTCAE term. TEAEs are defined as those AEs with a start or worsening date on or after the start date of study treatment until 47 d after the end date of study treatment (that is, on-T period). SAEs starting or worsening after the on-T period, if reported as related to the study treatment, were also counted as TEAEs. Proportions of treatment discontinuation, interruptions and dose reductions due to any AEs were also described. All potential cases with ILD were reviewed by an independent ILD adjudication committee. Data management was performed using TrialMaster software compliant with 21 CFR Part 11. The same software was used for patient registration. Continuous variables were presented by their mean and s.d. or median and IQR and categorical variables as percentages. All enrolled patients received at least one dose of study drug so that the full analysis set and safety analysis set correspond to the same population. Exploratory analyses were performed to assess the association between BL and dynamic biomarkers on ORR and PFS through logistic and Cox's regression models. To assess the assumption of linearity, splines were used. All additional tests beyond the primary test were two sided; R/SAS 9.4 was used for all analyses. DEG of RNA-seq data was performed using R packages Deseq2 and glmmseq and the Benjamini–Hochberg method was used to control for the false discovery rate ($P_{adj} < 0.05$). The study protocol was amended on 15 April 2022 to include patients with tumors presenting any HER3-membrane expression level at study entry and, thereafter, on 26 November 2024 to add a central review of RECIST response.

### HER3 and HER2 staining and spatial profiling

HER3 staining was centrally performed on 72 samples by Roche CDx CAP/CLIA Laboratory (Tucson) using clone SP438 and scored as follows: membrane *H*-score: 0–300; cytoplasm *H*-score: 0–300; overall membrane positivity at ×10 magnification: 0–100. Overall, 4 samples at baseline were not available (not provided by the participating centers) and 23 samples were excluded from the analysis due to tumor cellularity <10%. Centralized HER2 assessment on tumor biopsies at BL was performed by a GEFPICS (Groupe d'Etude des Facteurs Pronostiques par Immunohistochimie dans le Cancer du Sein)-trained pathologist using the Roche HER2 (4B5) clone and scored according to the last version of the American Society of Clinical Oncology (ASCO) and College of American Pathologists (CAP) guidelines[39]. 'Ultralow' HER2 category

was defined as cases showing a faint-to-weak, incomplete membrane staining in <10% of tumor cells (classified in the IHC 0 category following the ASCO and CAP guidelines). A total of 69 samples was available for centralized HER2 assessment, because 4 samples were not provided and the remaining 26 had insufficient tumor tissue for further analysis.

Pairs of H&E and IHC slides stained for HER3 expression were collected at BL and analyzed by machine learning algorithms to identify primary markers of resistance. On the pathologist's review, 69 pairs containing sufficient tumor tissue and TME were selected for analysis.

We first reproduced the analysis of target spatial distribution on the IHC slides as performed in the DAISY clinical trial[14]. The same preprocessing operations were used to delineate the tissue of interest within annotations provided by an expert pathologist, highlighting tumor tissue and its surrounding environment. Nonoverlapping patches of size 80 × 80 pixels$^2$ were extracted to account for the different resolution at which the slides were scanned in our study. Patches with >60% of red, green and blue values <2 and 90% of red, green and blue values >240 were identified as black and white patches and discarded. Two different models were employed to extract representations from the patches: the same model used in the Daisy clinical trial and the CONCH model[40]. Using the Davies–Bouldin index, we determined an optimal number of clusters to be seven for the DAISY-like embeddings and eight for the CONCH embeddings for a number of clusters ranging from seven to twelve. Subsequently, we applied the mini-batch *K*-means algorithm to these optimal cluster numbers and computed the cluster percentages.

To further integrate tissue microenvironment in the analysis, we aimed to leverage the information available from both H&E and IHC slides. To this end, we first extracted microenvironment features from the H&E slide using the CellViT model[41]. Specifically, we employed the CellViT-SAM-H model with HoVer-Net decoder[42] trained on the Pannuke dataset[43] to segment and classify nuclei into five classes: neoplastic, epithelial, inflammatory, connective and dead.

To incorporate HER3 expression, we registered the H&E slide onto the IHC slide. The slides were serialized, with a difference of up to 15 µm between H&E and IHC slides, providing a solid foundation for joint modality analysis. To perform registration, we relied on the VALIS registration pipeline[44]. Originally developed on surgical cuts, we adapted the method for biopsy slides with several preprocessing steps.

Initially, we identified the tissue regions on the slides that could be registered. These regions were then cropped to ensure the same scale on both modalities. The resulting images were subsequently processed using a preprocessing operator based on color deconvolution from a *K*-means clustering, with adaptive histogram equalization. Due to the noisy nature of the clustering results, we ran the VALIS pipeline on three different seeds and retained the seed with the best rigid registration error provided by the method. We finally computed the micro-nonrigid registration on 25% of the full-resolution whole-slide imaging. After registration, we identified six pairs of slides with a relative target registration error above one, which we considered too high to be exploitable in our next analysis. We excluded these slides and extracted nonoverlapping 128 × 128 pixel$^2$ patches from the remaining H&E slides. Black and white patches were discarded and warped onto the IHC slide using the coordinates of the top left corner through the trained registration models produced by the VALIS pipeline. To ensure that the patches contained relevant information, we removed any that fell outside the tissue contours of the IHC slide after registration.

For feature extraction, we performed the following steps: from the H&E slide, we extracted the number of cells for each class and computed several morphological features (area, perimeter, compactness, roundness, solidity and elongation) averaged across each class within each patch. From the IHC slide, we measured the distribution of DAB staining (mean, s.d., minimum, maximum and median $q1$ and $q3$ values) on the corresponding registered patch. The feature vectors from both modalities were concatenated, normalized and fed into a *K*-means algorithm, after which we computed cluster percentages on each slide. We switched to the Calinski–Harabasz score to identify the optimal number for clusters because it provided a more precise indication in this case. For a number of clusters ranging from 7 to 12, we identified an optimal number of 8 clusters. The same analysis was performed on the features obtained from the H&E slides exclusively, where we identified an optimal number of ten clusters. Unlike the DAISY-like analyses, this process did not require a pathologist's annotations due to the additional information available from the H&E slides. For all these analyses, using R v.4.1.2, we applied Dirichlet's regression to identify which clusters were significantly associated with the objective response to treatment. Statistical significance was assessed using Wald's test based on Dirichlet-distributed parameters. The second analysis involved investigating HER3 distribution within TCs. First, we segmented the nuclei on the IHC slides by extracting patches of size 512 × 512 pixels$^2$ with an overlap of 20 µm and removed black and white patches. Then, we employed SOP[45] on the extracted patches to retrieve nuclei segmentation using the same training protocol applied in the DAISY trial. Overlapping nuclei with >50% overlap were merged. A contrast correction operation was applied to enhance nuclei segmentation, involving clamping values >0.3 and rescaling the value within this new range. The resulting nuclei segmentation was then exported to QuPath v.5.0.0 (ref. 46). We used the provided tools to estimate stain decomposition vectors and cell membranes and to measure staining distribution within the segmented cells. For the stain decomposition vectors, we estimated the vectors from the first slide of the stack and applied the same values for every slide. For estimating the cell membranes, we used the provided cell expansion tool with a limit at 20 pixels from nuclei boundaries. Finally, we removed negative cells and/or cells with a background detected in the cytoplasm and mean DAB cytoplasm optical density variance across the cells for each patient. To identify negative cells, we trained a *K*-means algorithm to delineate two clusters from DAB optical density average value in the detected cells over all the slides and set the threshold at the average between the two detected centroids. We compared the distribution of this value between nonresponders and responders using a Mann–Whitney *U*-test. Finally, among the 63 slides used to compute the clustering, 48 were compared with slides stained for ERG expression. Using QuPath software, we identified positive and negative cells within these slides. The absolute number of ERG$^+$ cells in analyzed tissue was then compared with the number of patches belonging to each cluster for each patient with Spearman's correlation test and *P* values adjusted for multiple hypothesis testing using the Benjamini–Hochberg method.

### Genomic and transcriptomic analysis

The tumor samples were qualified for WES and bulk RNA-seq if the sample contained ≥10% and 30% TCs, respectively. In total, 43 frozen tumor biopsies at baseline were analyzed for WES and 43 blood samples were used as germline control. Overall, at baseline, 15 fresh biopsies were either not collected or not provided by the participating centers, 28 were excluded due to <200 ng of DNA or <10% TCs and 13 failed the quality control. Then 22 pairs of baseline or on-T frozen tumor biopsies were analyzed for bulk RNA-seq ($n$ = 12 at C1D3, $n$ = 4 at C1D19 and $n$ = 6 at C2D3). At BL, 15 fresh biopsies were not provided by the participating centers, 28 were excluded due to <200 ng of RNA or <30% TCs, 5 failed the quality control and 29 did not have the matched on-T sample. On-T, 22 fresh biopsies were unavailable because they were either not provided or not collected by the participating centers, 39 were excluded due to <200 ng of RNA or <30% TCs, 1 sample failed the quality control and 15 did not have the matched BL sample.

**DNA and RNA extraction.** DNA and RNA extraction Genomic DNA was isolated from blood using the DNeasy Blood and Tissue Kit (QIAGEN, cat. no. 69504), according to the manufacturer's guideline. DNA or RNA dual extraction from the tissue biopsy was done using the Allprep

DNA/RNA Micro kit (QIAGEN, cat. no. 80284) to purify DNA along with TRIzol LS Reagent (Thermo Fisher Scientific, cat. no. 10296028) to purify RNA. In brief, after homogenizing the biopsy cells, the lysate was passed through the Allprep DNA spin column provided by the kit. After centrifugation at 8,000*g* for 30 s, the DNA kept in the column filter was used for DNA purification while the flow-though was used for RNA purification using the TRIzol LS Reagent, according to the manufacturers' guidelines.

**Low-input exome.** The DNA quality was checked on the Agilent Fragment Analyzer (Agilent Technologies) and the quantity was determined using Qubit dsDNA Broad Range Assay (Invitrogen, cat. no. Q32853). Genomic DNA, 200 ng, was sheared with the Covaris E220 system (LGC Genomics or Kbioscience) to obtain 150-bp fragments according to the manufacturer's instructions. Briefly, DNA fragments were end-repaired, extended with an 'A' base on the 3′-end, ligated with paired-end adapters with the Bravo Platform (Agilent Technologies) and amplified to generate libraries (ten cycles). Hybridization-based exome enrichment was performed using the Agilent SureSelectXT Low Input Clinical Research Exome v.2 target enrichment system (Agilent Technologies). The final libraries were indexed, pooled and sequenced using the onboard cluster method, as paired-end sequencing (2× 100 bp) on an Illumina NovaSeq-6000 sequencer at Gustave Roussy.

**Bulk RNA-seq.** The RNA integrity (RNA integrity score ≥2.0) was checked on the Agilent Fragment Analyzer (Agilent Technologies) and the quantity was determined using Nanodrop. A SureSelect Automated Strand Specific RNA Library Preparation Kit was used according to the manufacturer's instructions with the Bravo Platform (Agilent Technologies). Briefly, 200–300 ng of total RNA per sample was used for poly(A) messenger RNA selection using oligo(dT) beads and subjected to thermal mRNA fragmentation. The fragmented mRNA samples were subjected to complementary DNA synthesis and further converted into double-stranded DNA using the reagents supplied in the kit; the resulting double-stranded DNA was used for library preparation. The final libraries were indexed, purified, pooled together in equal concentrations and subjected to paired-end sequencing (2× 100 bp) on a Novaseq-6000 sequencer (Illumina) at Gustave Roussy.

### Bioinformatic analyses

**WES.** Point mutations, small indels and copy-number alterations (CNAs) were detected using an end-to-end pipeline on the raw WES files. In brief, paired-end reads were controlled (FastQC v.0.11.8), trimmed (Fastp v.0.20)[47] and aligned to the reference human genome GRCh37 (BWA-MEM v.0.7.17)[48]. Files with aligned reads were processed following the best practices of GATK bundle v.4.1.8.1. Processed and aligned reads were then used as input to mutation- and CNA-calling algorithms. As advised in GATK guidelines, we used a 'panel of normal' to remove artifactual or false-positive mutations recurrently found in normal blood samples. Point mutations and small indels were called using Mutect2 (ref. 49) and the panel of normal. All putative variants identified by Mutect2 were first filtered to account for possible sample contamination and read orientation artifacts. Additional threshold- and rule-based filtering was applied to the read coverage, genomic position and variant allele frequency.

After all the filtering, 6,608 somatic point mutations and small indels were considered in the analysis of the 43 WES samples. CNA, tumor purity and average tumor ploidy were identified with the FACETS R package v.0.5.14 (ref. 50) run with parameters cval_pre = 25 and cval_pro = 500. To mitigate the effect of segmentation errors, only gene CNAs arising from segments spanning <10 Mb were considered in downstream analyses. Each CNA was classified into one of six categories and only high-level focal amplifications or homozygous focal deletions were considered. CNAs were categorized into five classes, with thresholds adjusted for the presence of whole-genome duplication (WGD): high-level gain was defined as six or more copies without WGD or ten or more copies with WGD; medium-level gain as four to five copies without WGD or seven to nine copies with WGD; low-level gain as three copies without WGD or five to six copies with WGD; homozygous deletion as zero copies; and loss of heterozygosity as one to two copies overall and zero copies for the minor allele without WGD, or one to four copies overall and zero copies for the minor allele with WGD. Oncogenic events were identified by intersecting point mutations and small indels with the OncoKB[51] database and gene amplifications or deletions with the OncoKB or CIViC[52] databases.

Point mutations from all 43 WES samples were summarized into a matrix of mutation counts with 96 rows for the 96 trinucleotide mutation categories, totaling 6,280 point mutations. Only samples with at least 50 detected somatic point mutations were used for the mutational signature analysis, resulting in the selection of 36 out of 49 samples with WES data available. Mutational signature activities in each sample were determined by projecting this matrix onto a shortlist of reference signatures from the SBS signatures COSMIC v.3.2 database. The shortlist was established by downloading known signature activities in The Cancer Genome Atlas and Pancancer Analysis of Whole Genomes cohorts (available at https://www.synapse.org/Synapse:syn11804065) and selecting signatures showing an activity in at least 2% of breast cancer samples in any of the two cohorts, or of particular interest to our cohort (signatures SBS31, SBS35, SBS44 and SBS90). Overall, 21 signatures were selected and used as a reference set to perform the deconvolution using MutationalPatterns R package[53] v.3.12.0. In an effort to mirror the original SigProfiler algorithm used for deconvoluting mutational signatures, we used the part of the Julia code (https://bitbucket.org/bbglab/sigprofilerjulia) that implements the SigProfiler algorithm from ref. 54 to run the sparsity-inducing step occurring after a first signature activity assignment by non-negative matrix factorization.

**Bulk RNA-seq.** Raw Illumina reads were demultiplexed using bcl2fastq v.2.20 (https://support.illumina.com/sequencing/sequencing_software/bcl2fastq-conversion-software.html). Quality control of reads was performed with fastQC v.0.11.8 (https://www.bioinformatics.babraham.ac.uk/projects/fastqc) and contamination assessment with Fastq_Screen v.0.15.3 (https://zenodo.org/doi/10.5281/zenodo.1344583) against the default genomes database. All quality control reports were aggregated using MultiQC v.1.14 (ref. 55). Bad sequence quality and adapter trimming was performed using fastp v.0.23.2 (ref. 47). Transcript-level quantification was performed using Salmon v.1.4.0 (ref. 56) with the reference human genome hg38.101. Sample-level quantification were aggregated using the tximport v.1.32.0 (https://bioconductor.org/packages/release/bioc/vignettes/tximport/inst/doc/tximport.html) package on R v.4.4.1. Genes that had fewer than five counts for any of the compared condition levels were discarded. DEAs were performed using the DESeq2 (ref. 57) package v.1.44.0. Differential analyses using an interaction term were performed using the glmmSeq (https://cran.r-project.org/web/packages/glmmSeq/vignettes/glmmSeq.html) R package v.0.5.5, GSEA, clusterProfiler v.4.12.0 package and multiple term databases in their latest version (MSigDb v.7.1, WikiPathways, KEGG, Reactome, DisGenet, Disease Ontology, Gene Ontology, Network of Cancer Genes). All *P* values from any statistical test performed were false recovery rate adjusted using the Benjamini–Hochberg method[58]. To investigate the prognostic signature for PFS, we used *z*-scores to avoid the influence of highly expressed genes. We used transcriptomic data obtained by RNA bulk analyses from 50 frozen biopsies at BL after passing quality control. We performed univariate Cox's proportional hazard models for each transcription factor using the Survival package in R. We generated a prognostic signature, using an adaptive lasso method with a preliminary step in the model subject to the ridge penalty. A 5× crossvalidation was used to determine the optimal value of $\lambda$. We repeated the

adaptive lasso selection 100× and selected the transcription features with repeated occurrence frequencies >80%. The analysis were performed using R package biospear[59]. PAM50 molecular subtypes were determined using normalized transcriptomic data transcripts per million through the following steps.

*Extraction of PAM50 genes*. The 50 genes comprising the PAM50 signature were extracted from the normalized transcripts per million expression matrix for each sample. PAM50-specific normalization: given that all samples in our cohort were $HR^+HER2^-$, a tailored normalization approach was applied, as recommended for subtype prediction in this specific context (the normalization was performed using the publicly available code: https://github.com/afernan4/PAM50_ER_HER2_normalization). Application of the PAM50 predictor: after normalization, the PAM50 predictor was applied using the original method and code available at: https://genome-publications.bioinf.unc.edu/PAM50.

### Characterization of the tumor and TME by IMC

We analyzed, using IMC, 61 samples at BL and 57 on-T. At baseline, 4 samples were not available because they were not provided by the participating center, 6 samples were excluded for insufficient tumor cellularity (0%) and 28 were nonanalyzable due to inadequate tumor staining (technical issues). On-T, 30 samples were not available because either they were not provided by the participating centers or biopsies were not collected and 12 samples were nonanalyzable due to inadequate tumor staining (technical issues).

**Antibody selection.** All antibodies used in IMC were first validated by immunofluorescence using breast and lung cancer tissues to determine optimal staining and specificity. Note that the anti-DXd antibody selectively binds the DXd moiety linked to the antibody and does not bind the payload detached from the antibody, because the free unbound DXd is washed out during processing of the samples and only DXd bound to the antibody can still be detected. Validated antibodies were conjugated to metal isotopes and tested by IMC to ensure staining specificity and intensity. They were then further validated in multiplexed IMC experiments and optimal concentrations of all metal-conjugated antibodies were determined by analysis of IMC images in breast cancer tissues (Supplementary Table 5).

**Antibody conjugation.** Metals were conjugated to antibodies according to the manufacturer's instructions (Maxpar X8 Antibody Labeling Kit). Metal-tagged antibodies were stored in a Candor Antibody Stabilizer (Candor Biosciences) at 4 °C.

**Tissue labeling.** FFPE tumor slides were cut at 5 mm and incubated at 60 °C for 2 h before they were dewaxed in xylene, rehydrated in 100% alcohol and washed in water. Tumor tissues were incubated in antigen retrieval (Tris-EDTA, pH 9.0, 96 °C for 30 min) and left on the bench for 30 min to cool down. Next, slides were washed in water, then in phosphate-buffered saline (PBS), before blocking with 3% bovine serum albumin in PBS for 45 min and incubation with metal-tagged antibodies overnight at 4 °C. They were incubated with the remainder of the metal-tagged antibodies overnight at 4 °C. Subsequently, slides were washed with PBS and 0.1% Triton, then they were incubated with Cell-ID intercalator-Ir 125 µM diluted in PBS and 0.5% bovine serum albumin for DNA detection (Fluidigm, cat. no. 201192A) for 5 min. Finally, slides were washed with water and air dried. To facilitate a comprehensive analysis, the pathologist marked the regions of interest (ROIs) on each slide. Hence, three ROIs were identified on each slide and then delineated using the IMC (Supplementary Fig. 10).

**IMC acquisition process.** Before the acquisition, the Hyperion mass cytometry system IMC was auto-tuned using a three-element tuning slide according to the tuning protocol provided by Standard BioTools. ROIs with sizes of 1 $mm^2$ (1,000 × 1,000 $µm^2$) were ablated and acquired at 200 Hz. For each sample, one to three ROIs were defined for the acquisition on Hyperion. The data obtained from each scanned spot, where each antibody corresponded to a single image per sample, were processed. These individual images were then combined to create a multi-image stack.

**Image analysis pipeline.** Raw data were visualized and converted to tiff format using the Standard BioTools MCDTM viewer. Next, ROIs were converted to TIFF concatenated images using Fiji software and cell segmentation was performed on the iridium channel for each ROI of each patient using the Qupath Stardist module. This segmentation process allowed the identification of individual cells and the extraction of single-cell distribution information. Using QuPath, a training image composed of several images from the dataset was used to classify regions and cell phenotypes. To discriminate the tumor region from the stroma, a pixel classifier tool was trained on a pan-cytokeratin marker. Then, to classify each cell population, an object classifier tool was trained by manually selecting positive and negative cells. The random Forest algorithm was applied to classify these detections (Supplementary Fig. 10). In addition, spatial analysis was conducted to explore the interaction between immune cells and TCs.

### CTC analysis

**Blood sample collection.** The study was designed to collect circulating TCs (CTCs) from the first 35 patients enrolled at the Gustave Roussy Cancer Center.

**CTC enumeration by CellSearch.** CTCs were enumerated using CellSearch (Menarini Silicon Biosystems) on 7.5 ml of blood according to the manufacturer's protocol as previously described[60]. Using CellSearch, we obtained CTC count data for 36 patients, with 22 having CTC assessments at each time point.

**CTC enrichment, immunofluorescence staining and isolation.** Blood samples, 28 ml, were collected in CellSave tubes (Menarini Silicon Biosystems). Negative selection of CTCs was performed using the RosetteSep Human CD36 Depletion Cocktail (STEMCELL Technologies, cat. no. 15167) according to the manufacturer's protocol as previously reported[61–63]. The enriched cell fraction was washed with 1× PBS and centrifuged for 5 min at 558*g*. The cell pellet was suspended in 100 µl of fixative solution medium A from the Fix&Perm kit (Thermo Fisher Scientific, cat. no. GAS004) and washed with 1× PBS (5 min, 368*g*). After centrifugation the cell pellet was resuspended with 100 µl of permeabilization solution medium B from the Fix&Perm kit and anti-HER3 monoclonal antibody (2 µg $ml^{-1}$, Thermo Fisher Scientific, clone RTJ2, cat. no. MA1-860), and incubated for 20 min at room temperature. After a 1× PBS wash the secondary goat anti-mouse AF488 antibody (Life Technologies, cat. no. A11029, 1:800) and 50 µl of staining reagent containing cytokeratin (CK)-phycoerythrin (CK 8, 18 and 19) and CD45-allophycocyanin antibodies (Menarini Silicon Biosystem, cat. no. 7900001) were added (dilution 1:6). The cell suspension was incubated for 20 min in the dark at room temperature. After a 1× PBS wash, the cell pellet was resuspended in 300 µl of 1× PBS and kept at +4 °C. Hoechst 33342 (16.7 µg $ml^{-1}$, Sigma-Aldrich, cat. no. 14533-100MG) was added before cell sorting. Individual CTC isolation was performed using a BD FACS ARIA III cell sorter (BD Biosciences) equipped with four lasers (405 nm, 488 nm, 561 nm and 640 nm). The system was run at 138 kPa pressure, a 100-µm nozzle and yield precision mode. Cell sorting was started by gating $Hoechst^+$ elements. The second gate enabled selection of $CD45\text{-}APC^-$ events. Three populations, including $Hoechst^+CD45^-CK^+HER3^-$, $Hoechst^+CD45^-CK^+HER3^+$ and $Hoechst^+CD45^-CK^-HER3^+$ cells, were sorted and collected in a 96-well plate. As a control, 20 $Hoechst^+CD45^+CK^-HER3^-$ cells were sorted. Plates were centrifuged 10 min at 280*g* and frozen at −20 °C for at least 30 min.

For FACS, CTC count data were available for 34 patients, with 27 having 3 assessments at different time points.

### Reporting summary

Further information on research design is available in the Nature Portfolio Reporting Summary linked to this article.

## Data availability

De-identified clinical data can be requested by filling out the data request form for Gustave Roussy's clinical trials at https://redcap.link/DataRequestClinicalTrialsGustaveRoussy. The steering committee and the sponsor will review the requests on a case-by-case basis. The anticipated timeframe for response is about 2 weeks. In case of approval, a specific agreement between the sponsor and the researcher may be required for data transfer.

## Code availability

De-identified whole-genomic and transcriptomic data and digital pathology data have been deposited to the European Genome–phenome Archive (accession no. EGAD50000000773). Digital pathology data are available via GitHub at https://github.com/gustaveroussy/ICARUS-01_Public. Other data that support the findings of this study are available from the corresponding author upon reasonable request.

## References


38. Schemper, M. & Smith, T. L. A note on quantifying follow-up in studies of failure time. *Controlled Clin. Trials* **17**, 343–346 (1996).
39. Wolff, A. C. et al. Human epidermal growth factor receptor 2 testing in breast cancer: ASCO–College of American Pathologists Guideline update. *J. Clin. Oncol.* **41**, 3867–3872 (2023).
40. Lu, M. Y. et al. A visual-language foundation model for computational pathology. *Nat. Med.* **30**, 863–874 (2024).
41. Hörst, F. et al. CellViT: vision transformers for precise cell segmentation and classification. *Med. Image Anal.* **94**, 103143 (2024).
42. Graham, S. et al. Hover-Net: simultaneous segmentation and classification of nuclei in multi-tissue histology images. *Med. Image Anal.* **58**, 101563 (2019).
43. Gamper, J., Alemi Koohbanani, N., Benet, K., Khuram, A. & Rajpoot, N. in *Digital Pathology* (eds Reyes-Aldasoro C. C. et al.) 11–19 (Springer, 2019).
44. Gatenbee, C. D. et al. Virtual alignment of pathology image series for multi-gigapixel whole slide images. *Nat. Commun.* **14**, 4502 (2023).
45. Le Bescond L., et al. Unsupervised nuclei segmentation using spatial organization priors. In *Medical Image Computing and Computer Assisted Intervention* (eds Wang, L. et al.) 325–335 (Springer Nature Switzerland, 2022).
46. Bankhead, P. et al. QuPath: open source software for digital pathology image analysis. *Sci. Rep.* **7**, 16878 (2017).
47. Chen, S., Zhou, Y., Chen, Y. & Gu, J. fastp: an ultra-fast all-in-one FASTQ preprocessor. *Bioinformatics* **34**, i884–i890 (2018).
48. Cibulskis, K. et al. Sensitive detection of somatic point mutations in impure and heterogeneous cancer samples. *Nat. Biotechnol.* **31**, 213–219 (2013).
49. Li, H. & Durbin, R. Fast and accurate short read alignment with Burrows–Wheeler transform. *Bioinformatics* **25**, 1754–1760 (2009).
50. Shen, R. & Seshan, V. E. FACETS: allele-specific copy number and clonal heterogeneity analysis tool for high-throughput DNA sequencing. *Nucleic Acids Res.* **44**, e131 (2016).
51. Chakravarty, D. et al. OncoKB: a precision oncology knowledge base. *JCO Precis. Oncol.* https://doi.org/10.1200/PO.17.00011 (2017).
52. Krysiak, K. et al. A community approach to the cancer-variant-interpretation bottleneck. *Nat. Cancer* **3**, 522–525 (2022).
53. Manders, F. et al. MutationalPatterns: the one stop shop for the analysis of mutational processes. *BMC Genom.* **23**, 134 (2022).
54. Pich, O. et al. The mutational footprints of cancer therapies. *Nat. Genet.* **51**, 1732–1740 (2019).
55. Ewels, P., Magnusson, M., Lundin, S. & Käller, M. MultiQC: summarize analysis results for multiple tools and samples in a single report. *Bioinformatics* **32**, 3047–3048 (2016).
56. Patro, R., Duggal, G., Love, M. I., Irizarry, R. A. & Kingsford, C. Salmon provides fast and bias-aware quantification of transcript expression. *Nat. Methods* **14**, 417–419 (2017).
57. Love, M. I., Huber, W. & Anders, S. Moderated estimation of fold change and dispersion for RNA-seq data with DESeq2. *Genome Biol.* **15**, 550 (2014).
58. Benjamini, Y. & Hochberg, Y. Controlling the false discovery rate: a practical and powerful approach to multiple testing. *J. R. Statist. Soc. B* **57**, 289–300 (1995).
59. Ternès, N., Rotolo, F. & Michiels, S. biospear: an R package for biomarker selection in penalized Cox regression. *Bioinformatics* **34**, 112–113 (2018).
60. Farace, F. et al. A direct comparison of CellSearch and ISET for circulating tumour-cell detection in patients with metastatic carcinomas. *Br. J. Cancer* **105**, 847–853 (2011).
61. Pailler, E. et al. Acquired resistance mutations to ALK inhibitors identified by single circulating tumor cell sequencing in *ALK*-rearranged non-small-cell lung cancer. *Clin. Cancer Res.* **25**, 6671–6682 (2019).
62. Oulhen, M. et al. Circulating tumor cell copy-number heterogeneity in ALK-rearranged non-small-cell lung cancer resistant to ALK inhibitors. *npj Precis. Oncol.* **5**, 67 (2021).
63. Mezquita, L. et al. Resistance to BRAF inhibition explored through single circulating tumour cell molecular profiling in BRAF-mutant non-small-cell lung cancer. *Br. J. Cancer* **130**, 682–693 (2024).


## Acknowledgements

We thank all the patients, families, investigators and study personnel who participated in this study. We also acknowledge Daiichi Sankyo, for supporting this study and the whole ICARUS program. This work, as part of IHU PRISM National PRecISion Medicine Center in Oncology, also received state funding managed by the French National Research Agency under the France 2030 program (grant no. ANR-23-IAHU-0002). We are grateful to A. Fernandez-Martinez for her expert assistance and insightful contributions to the transcriptomic analysis.

## Author contributions

Leadership: B.P., F.A., D.S. and G.M. Study design: B.P., F.M., S.M., F.A., D.W.S. and D.S. Formal analysis: L.P., S.M., L.L., Y.P., B.J., A.A., C.C., E.B., Y.K., L.L., A.S. and F.S. Enrolled patients: B.P., F.M., G.N., C.V., J.S.F., V.D., F.D., T.B., A.D., M.A.B., D.L., D.M., E.D. and J.D. Lab analysis: F.M., N.C., N.D., D.T.N.T., S.B., F.M.C., F.F., M.O., P.K., G.M., B.P. and F.A. Imaging or pathology: M.L.T., L.L., N.S., K.G., H.T., M.V. and S.C. Data management: P.G., G.N. and R.C.H. Administration: R.C.H. and K.G. Editing and review: all authors.

## Competing interests

B.P. has received consulting fees from AstraZeneca (institutional), Seagen (institutional), Gilead (institutional), Novartis (institutional), Lilly (institutional), MSD (institutional), Pierre Fabre (personal) and Daiichi Sankyo (institutional or personal); research funding (to the institution) from AstraZeneca, Daiichi Sankyo, Gilead, Seagen and MSD; and travel support from AstraZeneca, Pierre Fabre, MSD, Daiichi Sankyo and Pfizer. F.M. has received consulting fees from Novartis and Pegascy. M.L.T. has received consulting fees from AstraZeneca and Daiichi Sankyo. J.S.F. has received consulting fees, honoraria for lectures and presentations and support for attending meetings

from and participation on data safety monitoring for AstraZeneca, GSK, Eisai, MSD, Lilly, Pfizer, Novartis, Daiichi Sankyo and Seagen. M.A.B. has received consulting fees from Daiichi Sankyo; honoraria for lectures and presentations from Exact Sciences; support for attending meetings from Novartis, Lilly and Seagen; and participation on data safety monitoring for MSD, AstraZeneca, Novartis, Lilly, Esai, Exact Sciences, Daiichi and Sankyo. T.B. has received grants or contracts from other entities, such as AstraZeneca (institution), Pfizer (institution), SeaGen (institution) and Novartis (institution); honoraria for lectures and presentations from SeaGen, Novartis, Pfizer and Lilly; support for attending meetings from Roche, AstraZeneca, Daiichi Sankyo, Pfizer and Novartis; and participation on data safety monitoring for AstraZeneca, Daiichi Sankyo, SeaGen, Novartis, Pfizer and Lilly. J.D. has received consulting fees from Daiichi Sankyo and AstraZeneca. A.S., F.S., L.L., D.W.S. and D.S. are employees of Daiichi Sankyo. S.M. is a data and safety monitoring member of clinical trials for IQVIA, Kedrion, Biophytis, Servier and Yuhan and a scientific committee study member of an observational study for Roche. F.A. has received research funding and speaker or advisor honoraria (compensated to the hospital) for Roche, AstraZeneca, Daiichi Sankyo, Pfizer, Novartis and Eli Lilly. The remaining authors declare no competing interests.

## Additional information

**Extended data** is available for this paper at https://doi.org/10.1038/s41591-025-03885-3.

**Supplementary information** The online version contains supplementary material available at https://doi.org/10.1038/s41591-025-03885-3.

**Correspondence and requests for materials** should be addressed to Barbara Pistilli.

**Peer review information** *Nature Medicine* thanks Aditya Bardia, Leif Ellisen and the other, anonymous, reviewer(s) for their contribution to the peer review of this work. Primary Handling Editor: Ulrike Harjes, in collaboration with the *Nature Medicine* team.

https://doi.org/10.1038/s41591-025-03885-3

a) Treatment outcome according to HER3-overall membrane positivity at 10x

| OVERALL MEMBRANE POSITIVITY | 25% | | | 25-75% | | | >75% | | |
|---|---|---|---|---|---|---|---|---|---|
| **Confirmed Response, N=72** | **N=16** | **%** | **95%CI** | **N=7** | **%** | **95%CI** | **N=49** | **%** | **95%CI** |
| **ORR** | 7 | 43.8 | [19.8;70.1] | 6 | 85.7 | [42.1;99.6] | 25 | 51.0 | [36.3; 65.6] |
| **CBR** | 7+1 | 50 | [24.7; 75.3] | 0 | 0 | [0;0.] | 25+7 | 65.3 | [50.3; 78.3] |
| Median PFS, months [95% CI] | 8.1 [4.4; NA] | | | 8.1 [6.7; NA] | | | 10.9 [8.2; 17.7] | | |

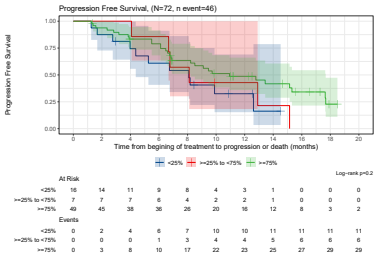


b)Treatment outcome according to HER3-membrane expression as measured by H-score

| MEMBRANE H SCORE | 0-100 | | | 100-200 | | | >200 | | |
|---|---|---|---|---|---|---|---|---|---|
| **Confirmed Response, N=72** | **N=16** | **%** | **95%CI** | **N=30** | **%** | **95%CI** | **N=26** | **%** | **95%CI** |
| **ORR** | 9 | 56.2 | [29.9;80.2] | 15 | 50 | [31.3; 68.7] | 14 | 53.8 | [33.4;73.4] |
| **CBR** | 9+1 | 62.5 | [35.4; 84.8] | 15+4 | 63.3 | [43.9;80.1] | 14+3 | 65.4 | [44.3; 82.8] |
| Median PFS [95%CI] | 6.7 [5.3; NA] | | | 9.1 [6.9; NA] | | | 10.9 [8.51; NA] | | |

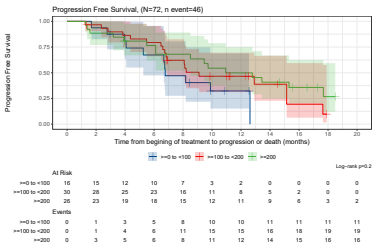


**Extended Data Fig. 1 | ORR and PFS according to HER3-membrane expression.** **a**. ORR and PFS according to HER3 membrane positivity as measured by overall membrane positivity at 10x and scored as < 25%, 25-75% and > 75% of tumor cells; **b**. ORR and PFS according to HER3 membrane positivity as measured by H-score 0-100, 100-200, ≥ 200; the 95% confidence interval was estimated using the Clopper–Pearson exact method.

https://doi.org/10.1038/s41591-025-03885-3

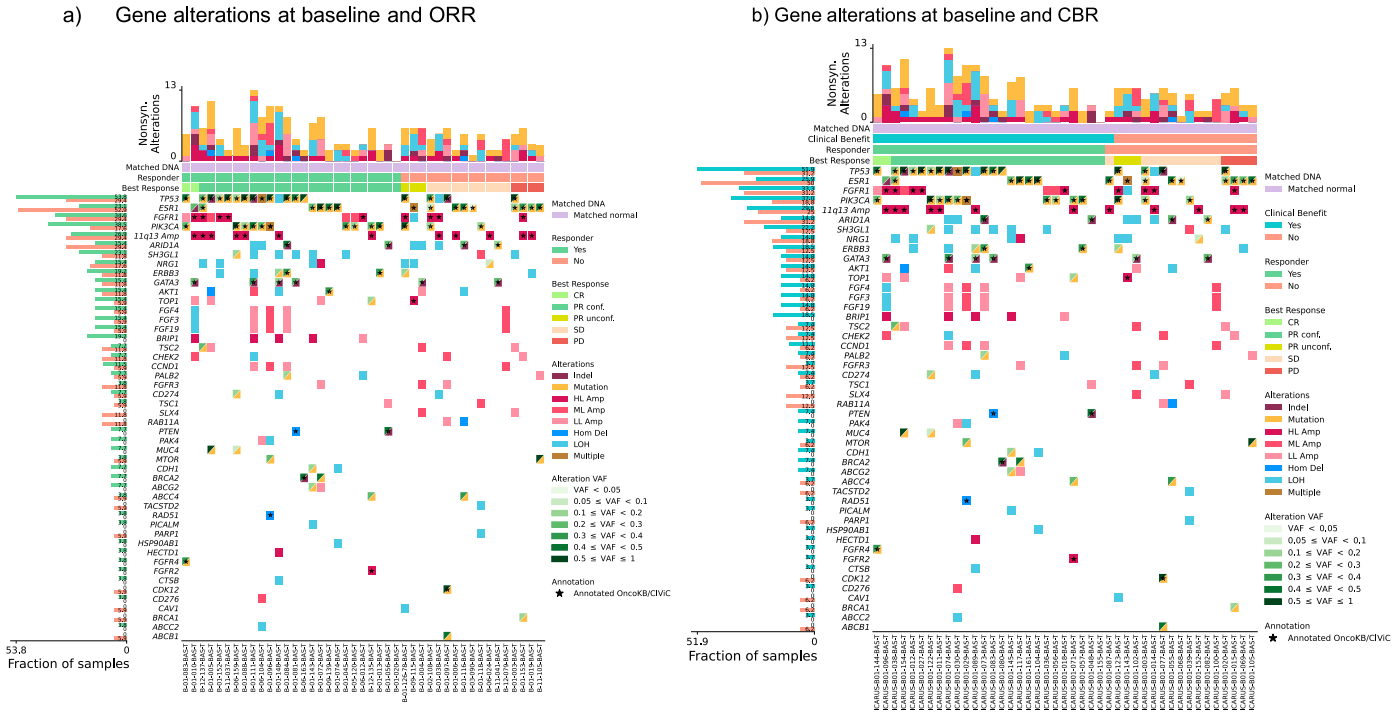


**Extended Data Fig. 2 | Gene alterations at baseline with response to HER3-DXd.** (**a**) Oncoplot showing non-synonymous point mutations, indels, homozygous deletions, loss of heterozygosity (LOH) and low, medium, and high-level amplifications in the set of 73 genes of interest, according to treatment response: responders (confirmed CR, PR), n = 26; non-responders (SD, PD, NE), n = 17.Blood samples were available for all patients. (**b**) Oncoplot showing non-synonymous point mutations, indels, homozygous deletions, loss of heterozygosity (LOH) and low, medium, and high-level amplifications in the set of 73 genes of interest, according to CBR: CBR (confirmed CR, PR, SD > 6 months; n = 27; non CBR (unconfirmed PR, SD < 6 months, PD; n = 16). Blood samples were available for all patients.

https://doi.org/10.1038/s41591-025-03885-3

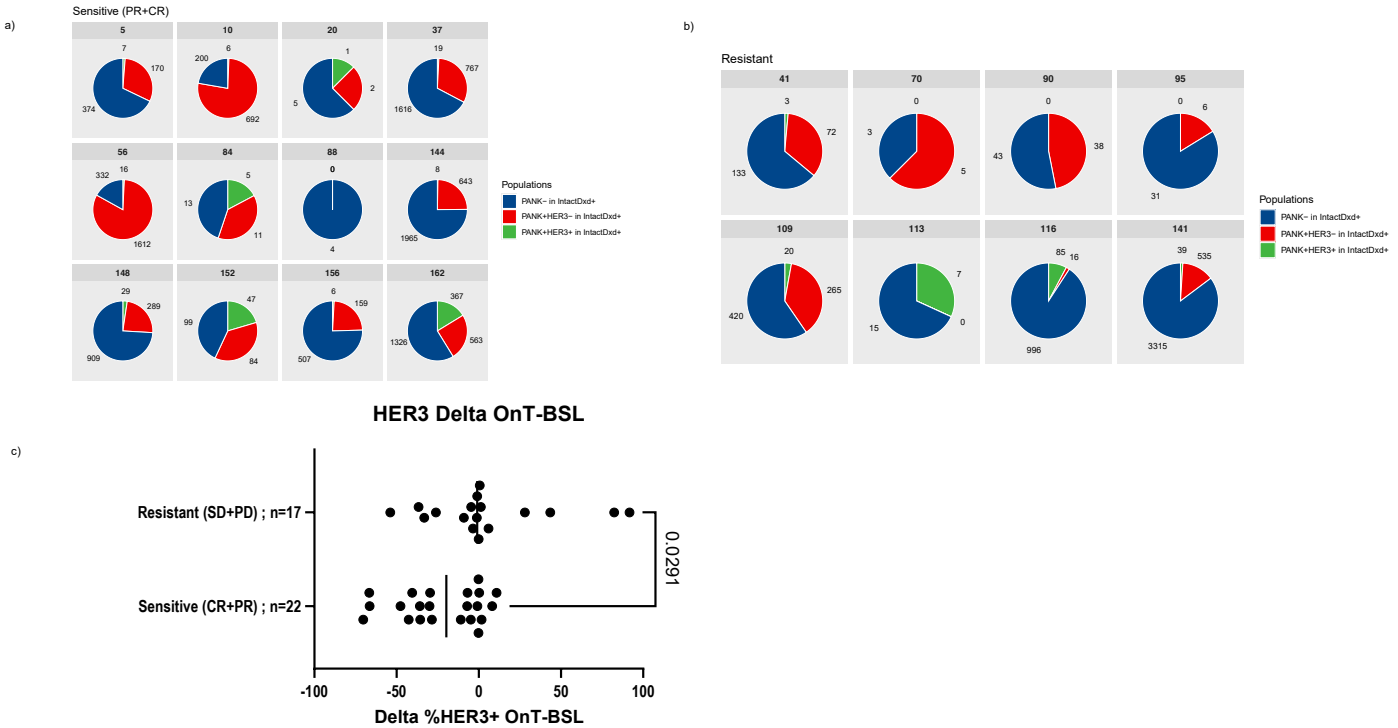


**Extended Data Fig. 3 | HER3-DXd interactions with tumor cells.** (**a, b**) Pie chart showing the proportion of the different cell phenotypes among the HER3-DXd-positive cells at C1D3 in responders (**a**) and non-responders (**b**); (**c**) Dynamics of HER3-positive cells after 1 or 2 doses of HER3-DXd in responders and non-responders (n = 39), showing a greater reduction on-treatment of HER3-positive cells in responders as compared to non-responders (Mann-Whitney U test, p-value 0.011).

https://doi.org/10.1038/s41591-025-03885-3

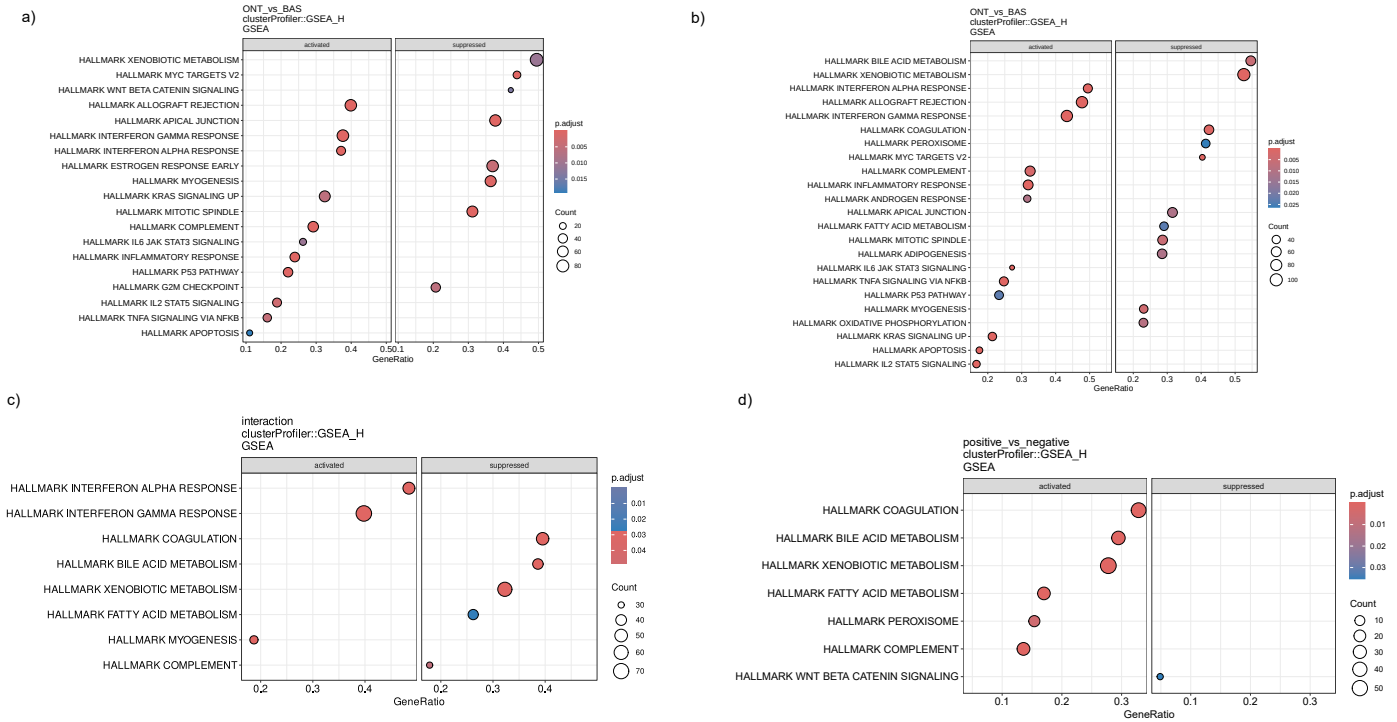


**Extended Data Fig. 4 | Genes and pathways modulated by HER3-DXd.** (**a, b**) Gene set enrichment analysis (GSEA), using the Hallmark gene set in the overall population (**a**) and in responders (**b**) showed upregulation of genes involved in immune response, particularly interferon alpha and gamma and complement signaling; (**c**) GSEA, using the Hallmark gene sets: Key activated/suppressed pathways in on treatment/baseline matched biopsies by comparing responders (n = 14 pairs) vs. non responders (n = 8 pairs), showing on-treatment activation of immune pathways in responders as compared non responders; (**d**) GSEA, using the Hallmark gene sets: Key activated/suppressed pathways in HER3-DXd-positive (HER3-DXd-positive cells ≥ 5%, n = 5) and HER3-DXd-negative tumors (HER3-DXd-positive cells < 5%, n = 7) on-treatment.

https://doi.org/10.1038/s41591-025-03885-3

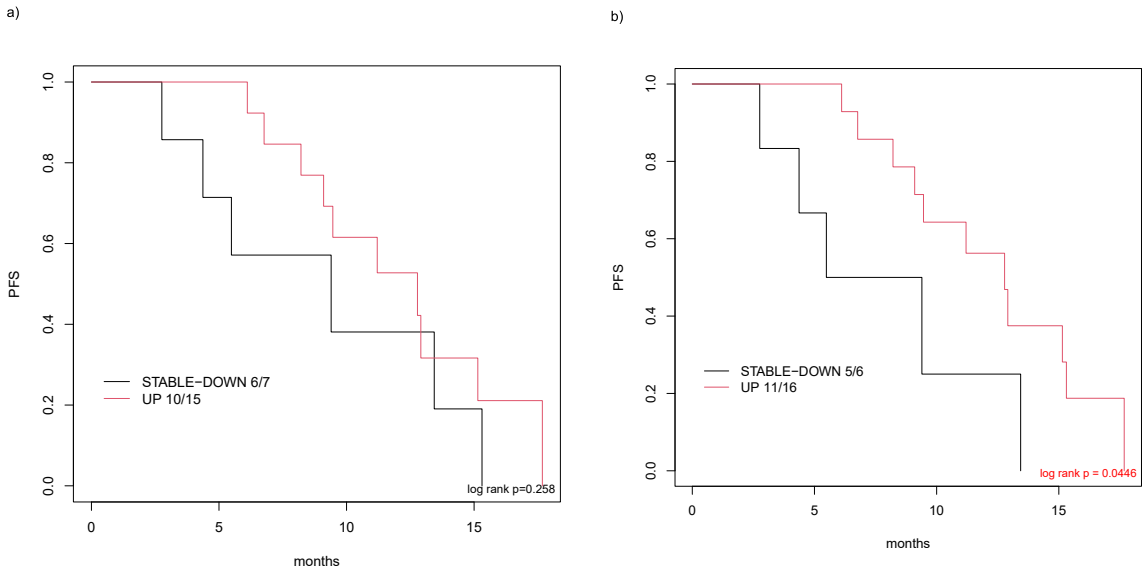


**Extended Data Fig. 5 | Interferon alpha and gamma signature and association with PFS.** (**a**) Kaplan-Meier curve estimating PFS according to up or stable/downregulation of interferon alfa (p-value = 0.258) (n = 22); (**b**) Kaplan-Meier curve estimating PFS according to up or stable/downregulation of interferon gamma (p-value = 0.045).

https://doi.org/10.1038/s41591-025-03885-3

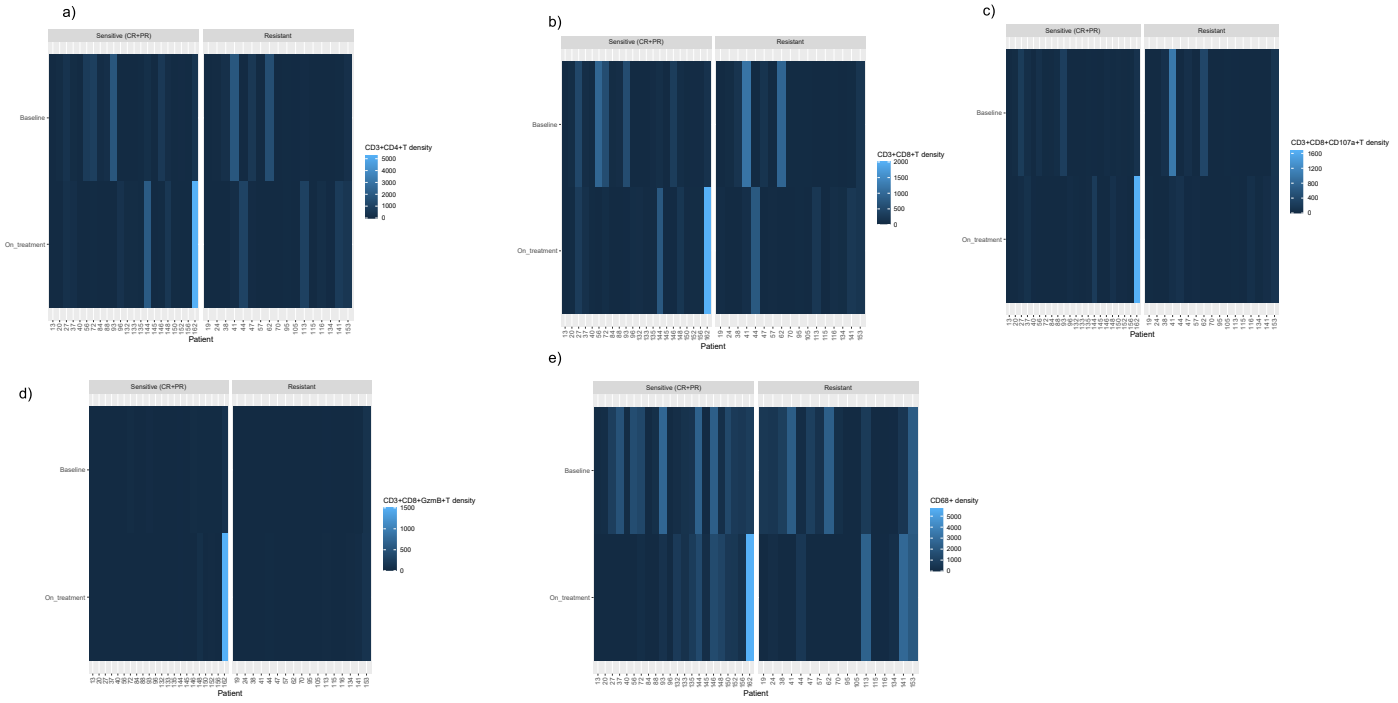


**Extended Data Fig. 6 | HER3-DXd interaction with the TME.** (**a**–**d**)Heatmaps showing density of CD4 + (**a**), CD8 + (**b**), C8 CD107a + (**c**) and CD8 GzmB+ cells (**d**) at baseline and on-treatment in matched samples of responders and non-responders; (**e**) Heatmaps showing density of CD68+ cells in responders and non-responders.

Corresponding author(s): Barbara Pistilli, MD

Last updated by author(s): Jun 10, 2025

# Reporting Summary

Nature Portfolio wishes to improve the reproducibility of the work that we publish. This form provides structure for consistency and transparency in reporting. For further information on Nature Portfolio policies, see our Editorial Policies and the Editorial Policy Checklist.

## Statistics

For all statistical analyses, confirm that the following items are present in the figure legend, table legend, main text, or Methods section.

| n/a | Confirmed |
|---|---|
| ☐ | ☒ The exact sample size (*n*) for each experimental group/condition, given as a discrete number and unit of measurement |
| ☐ | ☒ A statement on whether measurements were taken from distinct samples or whether the same sample was measured repeatedly |
| ☐ | ☒ The statistical test(s) used AND whether they are one- or two-sided<br>*Only common tests should be described solely by name; describe more complex techniques in the Methods section.* |
| ☐ | ☒ A description of all covariates tested |
| ☐ | ☒ A description of any assumptions or corrections, such as tests of normality and adjustment for multiple comparisons |
| ☐ | ☒ A full description of the statistical parameters including central tendency (e.g. means) or other basic estimates (e.g. regression coefficient) AND variation (e.g. standard deviation) or associated estimates of uncertainty (e.g. confidence intervals) |
| ☐ | ☒ For null hypothesis testing, the test statistic (e.g. *F*, *t*, *r*) with confidence intervals, effect sizes, degrees of freedom and *P* value noted<br>*Give P values as exact values whenever suitable.* |
| ☒ | ☐ For Bayesian analysis, information on the choice of priors and Markov chain Monte Carlo settings |
| ☒ | ☐ For hierarchical and complex designs, identification of the appropriate level for tests and full reporting of outcomes |
| ☐ | ☒ Estimates of effect sizes (e.g. Cohen's *d*, Pearson's *r*), indicating how they were calculated |

*Our web collection on statistics for biologists contains articles on many of the points above.*

## Software and code

Policy information about availability of computer code

| | |
|---|---|
| Data collection | An e-CRF with remote data entry was used for recording data required by the protocol and collected by the investigator.<br>Data management was performed using TrialMaster software compliant to 21 CFR Part 11. The same software was used for patient registration. |
| Data analysis | For WES: DNA quality was checked on the Agilent Fragment Analyzer (Agilent Technologies) and quantity was determined using QubitTM dsDNA Broad Range Assay (Invitrogen, cat. no. Q32853). For bulkRNAseq: The RNA integrity was checked on the Agilent Fragment Analyzer (Agilent Technologies) and quantity was determined using Nanodrop. SureSelect Automated Strand Specific RNA Library Preparation Kit was used according to manufacturer's instructions with the Bravo Platform (Agilent Technologies). For all statistical analysis we used R/SAS 9.4. In addition, for differential expression analysis of RNAseq data we used Deseq2 package v1.44.0 and glmmSeq R package v0.5.5.; and GSEA was done using clusterProfiler v4.12.0 package. For bioinformatic analysis on WES data we used FACETS R package v0.5.14; for Dirichlet regression analysis we used R version 4.1.2; for nuclei segmentation and ERG expression we used QuPath version 5.0.0; raw data from imaging mass cytometry were were visualized and converted to tiff format using the Standard BioTools MCDTM viewer v. 1.0.560.6.<br>The source to reproduce the analysis presented in the paper are available at: https://github.com/gustaveroussy/ICARUS_Public |

For manuscripts utilizing custom algorithms or software that are central to the research but not yet described in published literature, software must be made available to editors and reviewers. We strongly encourage code deposition in a community repository (e.g. GitHub). See the Nature Portfolio guidelines for submitting code & software for further information.

## Data

Policy information about availability of data

All manuscripts must include a data availability statement. This statement should provide the following information, where applicable:

- Accession codes, unique identifiers, or web links for publicly available datasets
- A description of any restrictions on data availability
- For clinical datasets or third party data, please ensure that the statement adheres to our policy

Data availability
De-identified clinical data clinical data can be requested by filling out the data request form for Gustave Roussy's clinical trials at https://redcap.link/DataRequestClinicalTrialsGustaveRoussy. Access to the data is restricted to protect participants' privacy and comply with clinical trial data protection regulations. The steering committee and the sponsor will review the requests on a case-by-case basis. The anticipated timeframe for response is about 2 weeks. In case of approval, a specific agreement between the sponsor and the researcher may be required for data transfer.

Code availability
De-identified whole genomic and trancriptomic data and digital pathology data have been deposited to the European Genome-phenome Archive (EGA) (EGA accession number EGAD50000000773). Other data that support the findings of this study are available from the corresponding author upon reasonable request. Digital pathology data are available at https://github.com/gustaveroussy.

## Research involving human participants, their data, or biological material

Policy information about studies with human participants or human data. See also policy information about sex, gender (identity/presentation), and sexual orientation and race, ethnicity and racism.

| | |
|---|---|
| Reporting on sex and gender | ICARUS BREAST 01 study allowed the inclusion of both female and male patients, however only female patients with advanced breast cancer were enrolled. |
| Reporting on race, ethnicity, or other socially relevant groupings | Collection of data on race and ethnicity is not allowed in France |
| Population characteristics | We included 99 patients with HR+/HER2- advanced breast cancer, who have progressed on prior CDK4/6inhibitors and have received one line of chemotherapy for ABC. Median age was 57.0 (48.0;66.0); median number of prior lines of therapy was 2 (1;4). |
| Recruitment | Patients were recruited according to predefined inclusion and exclusion criteria across 11 French sites. Patients were identified by medical oncologists and invited to participate to the study by local investigators if they met all eligibility criteria. Participation was voluntary and all participants provided a written informed consent before the enrollement. Selection bias was minimized by the rigorous application of study inclusion and exclusion criteria across all partecipating sites. |
| Ethics oversight | The protocol was submitted to the competent Ethics Commitee (CPP) which gave its approval on 12/03/2021. This study has also been approved by the Competent Authority on 29/04/2021 and was performed in accordance with the ethical principles of Declaration of Helsinki and consistent with the International Conference on Harmonisation Good Clinical Practice guidelines and other applicable regulatory requirements. A clinical study report will be written 1 year after the end of the study and send to CPP and other competent authorities. |

Note that full information on the approval of the study protocol must also be provided in the manuscript.

# Field-specific reporting

Please select the one below that is the best fit for your research. If you are not sure, read the appropriate sections before making your selection.

☒ Life sciences ☐ Behavioural & social sciences ☐ Ecological, evolutionary & environmental sciences

For a reference copy of the document with all sections, see nature.com/documents/nr-reporting-summary-flat.pdf

# Life sciences study design

All studies must disclose on these points even when the disclosure is negative.

| | |
|---|---|
| Sample size | 99 patients required to provide 85% power to test H0: ORR ≤ 12% at a one-sided 5% significance level, assuming ORR = 23% under the alternative |
| Data exclusions | 2 patients were not evaluable for ORR: one patient had only one tumor assessment with PR and then treatment was discontinued due to |

| | |
|---|---|
| Data exclusions | clinical progression, a second patient had a not evaluable global response of target lesions. For HER2 and HER3 staining: 4 samples at baseline were not available (not provided by the participating centers) and 23 samples were excluded from the analysis due to tumor cellularity < 10%. For WES analysis: 15 fresh biopsies were either not collected or not provided by the participating centers, 28 were excluded due to < 200 ng DNA or < 10% tumor cell and 13 failed the quality control. For bulkRNAseq: at baseline, 15 fresh biopsies were not provided by the participating centers, 28 were excluded due to < 200 ng RNA or < 30% tumor cell, 5 failed the quality control, 29 did not have the matched on-T sample; on-treatment, 22 fresh biopsies were not available because either not provided or not collected by the participating centers, 39 were excluded due to < 200 ng RNA or < 30% tumor cell, 1 sample failed the quality control, and 15 did not have the matched BL sample. For IMC: at baseline, 4 samples were not available because not provided by the participating center, 6 samples were excluded for insufficient tumor cellularity (0 %), 28 were non-analyzable due to inadequate tumor staining (technical issues); on-treatment, 30 samples were not available because either not provided by the participating centers or biopsies not collected, 12 samples were non-analyzable due to inadequate tumor staining (technical issues). For analysis of ERG expression at baseline, 48 samples at baseline were avalaible out of the 63 previously analyzed for HER3 expression by ML, 15 samples were no longer available for insufficient tumor tissue. For ML and WES analysis at progression, only 11 and 6 samples were available, respectively. Samples at progression from the partecipating sites had not been collected and analyzed yet, since 19 patients were still on treatment. |
| Replication | n/a (clinical trial) |
| Randomization | single arm open-label non-randomized phase II study |
| Blinding | Investigators were blinded to efficacy and exploratory analysis findings until statistical analysis have been completed. Investigators were not blinded to the group allocation for time of on-treatment tumor biopsy because it was not logistically possible and it did not affect data interpretation. |

# Reporting for specific materials, systems and methods

We require information from authors about some types of materials, experimental systems and methods used in many studies. Here, indicate whether each material, system or method listed is relevant to your study. If you are not sure if a list item applies to your research, read the appropriate section before selecting a response.

## Materials & experimental systems

| n/a | Involved in the study |
|---|---|
| ☐ | ☒ Antibodies |
| ☒ | ☐ Eukaryotic cell lines |
| ☒ | ☐ Palaeontology and archaeology |
| ☒ | ☐ Animals and other organisms |
| ☐ | ☒ Clinical data |
| ☒ | ☐ Dual use research of concern |
| ☒ | ☐ Plants |

## Methods

| n/a | Involved in the study |
|---|---|
| ☒ | ☐ ChIP-seq |
| ☒ | ☐ Flow cytometry |
| ☒ | ☐ MRI-based neuroimaging |

## Antibodies

| | |
|---|---|
| Antibodies used | HER3 staining was performed with Roche CDx CAP/CLIA Laboratory (Tucson) using clone SP438. HER2 staining was performed using VENTANA HER2/neu (4B5). CTC enrichment and staining was done using AF488 antibody (1/800, Life Technologies, #A11029) and CD45-APC antibody(Menarini Silicon Biosystem, #7900001) |
| Validation | The same HER3 antibody has been used across all clinical trials with HER3-DXd: Yu et al, JCO 2023; Krop et al, JCO 2023; Oliveira et al, Ann Oncol 2023. All antibodies used in imaging mass cytometry (IMC) were first validated by immunofluorescence using breast and lung cancer tissues to determine optimal staining and specificity. |

## Clinical data

Policy information about clinical studies

All manuscripts should comply with the ICMJE guidelines for publication of clinical research and a completed CONSORT checklist must be included with all submissions.

| | |
|---|---|
| Clinical trial registration | clinicaltrials.gov identifier NCT04965766 |
| Study protocol | Available with the manuscript |
| Data collection | From May 27th, 2021 to March 9th, 2023, 164 patients were screened, of whom 99 were enrolled to receive HER3-DXd 5.6 mg/kg IV every 3 weeks until progression or unacceptable toxicity. Patients were enrolled across the following French sites: Institut Paoli Calmettes, Marseille; Institut de Cancerologie de l'Ouest; Saint Herblain; Centre de Recherche en Cancérologie et Immunologie Nantes Angers, Nantes; Institut Régional du Cancer de Montpellier, Montpellier; Oncopole Claudius Regaud, Toulouse; Centre Léon Bérard, Lyon; Centre Antoine Lacassagne, Nice; Tenon Hospital, APHP, Paris; Curie Hospital, Paris; Centre Georges François Leclerc, Dijon; , Centre Hopital-Universitaire Limoges. |

Outcomes

The primary endpoint, objective response rate (ORR) was defined as the proportion of patients who achieved a confirmed complete response (CR) or partial response (PR), as assessed by local investigators, without initiation of new anticancer treatment. Confirmation of response had to be demonstrated with an assessment 4 weeks or later from the initial response. Treatment objective response was radiologically assessed every 6 weeks using RECIST V1.1. Secondary endpoints were: progression-free survival (PFS) by investigator assessment, duration of response (DOR), clinical benefit rate (CBR), overall survival (OS) and safety. Clinical benefit rate (CBR) was defined as the presence of at least a PR or CR, or a stable disease (SD) for six months or more under treatment. Kaplan-Meier estimations and curves were used to describe DOR, PFS and OS. PFS was defined as the time from the date of the first dose until documented disease progression or death from any cause, whichever occurs first. For patients without documented radiological progression, follow-up was censored at the date of last radiological assessment without progression, unless death occurs within 12 weeks following the date of last known progression-free, in which case the death was counted as a PFS event. DOR was calculated on the patients with either confirmed CR or PR and is defined as the time from the first documented confirmed CR or PR until the date of disease progression, or until the date of death. Safety endpoints (Adverse events (AEs), Adverse Events of Special Interest (AESIs), Serious Adverse Events (SAEs), Treatment-Emergent Adverse Events (TEAEs) and Treatment-Emergent probably related to treatment (TRAEs), defined by the National Cancer Institute Common Terminology Criteria for Adverse Events v 5.0 (NCI-CTCAE v5.0 ) were described as maximum grade for each patient by CTCAE Term.

## Plants

Seed stocks

n/a

Novel plant genotypes

n/a

Authentication

n/a